AD-A072 094 GEORGETOWN UNIV WASHINGTON D C DEPT OF PHYSICS F/G 20/1
INFLUENCE OF ABSORPTION ON NON-SPECULAR ULTRASONIC REFLECTIVITY--ETC(U)
JUL 79 T D NGOC, W G MAYER N00014-78-C-0584
UNCLASSIFIED GUUS-07791 NL

| OF |
AD A072094

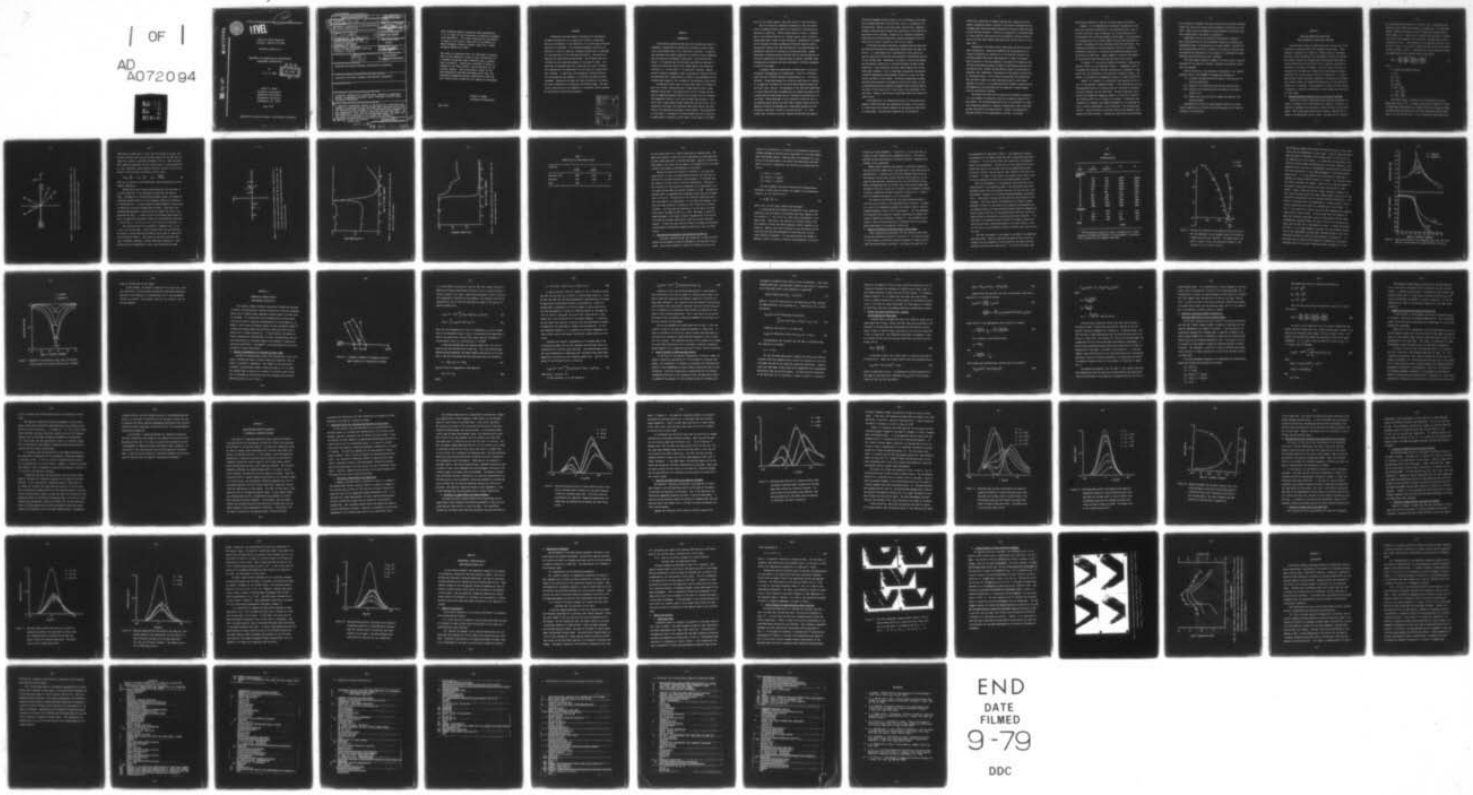

END
DATE FILMED
9-79
DDC

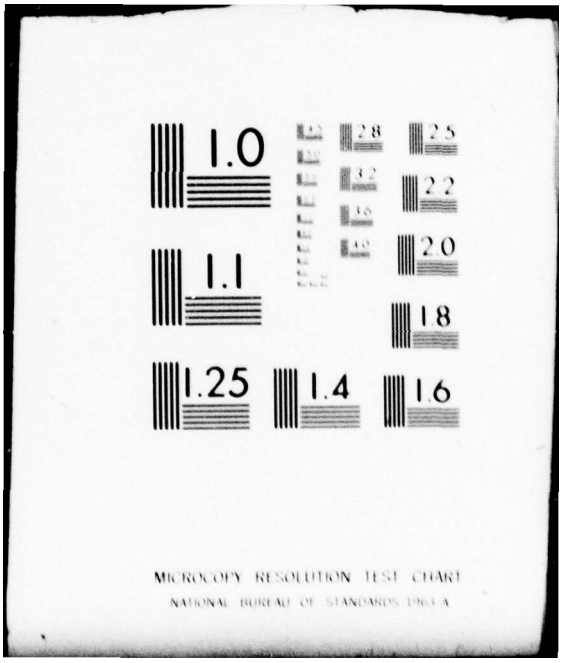
1.0
1.1
1.25
1.4
1.6
2.8
2.5
2.2
2.0
1.8
MICROCOPY RESOLUTION TEST CHART
NATIONAL BUREAU OF STANDARDS 1963 A

LEVEL II

Office of Naval Research
Contract N00014-78-C-0584

Technical Report No. 1

INFLUENCE OF ABSORPTION ON NON-SPECULAR ULTRASONIC REFLECTIVITY

by

T. D. K. Ngoc

Walter G. Mayer
Principal Investigator
Department of Physics
Georgetown University
Washington, DC 20057

July 1979

Unclassified

SECURITY CLASSIFICATION OF THIS PAGE (When Data Entered)

REPORT DOCUMENTATION PAGE	READ INSTRUCTIONS BEFORE COMPLETING FORM
1. REPORT NUMBER: GUUS-07791, TR-1	2. GOVT ACCESSION NO. / 3. RECIPIENT'S CATALOG NUMBER
4. TITLE (and Subtitle): Influence of Absorption on Non-Specular Ultrasonic Reflectivity	5. TYPE OF REPORT & PERIOD COVERED: Technical rept. 1 Sep 78 – 15 Jul 79 / 6. PERFORMING ORG. REPORT NUMBER
7. AUTHOR(s): T. D. K. Ngoc, Walter G. Mayer	8. CONTRACT OR GRANT NUMBER(s): N00014-78-C-0584
9. PERFORMING ORGANIZATION NAME AND ADDRESS: Physics Department, Georgetown University, Washington DC 20057	10. PROGRAM ELEMENT, PROJECT, TASK AREA & WORK UNIT NUMBERS: 121108
11. CONTROLLING OFFICE NAME AND ADDRESS: Office of Naval Research, Code 421, Arlington, Virginia	12. REPORT DATE: 23 July 1979 / 13. NUMBER OF PAGES: 76
14. MONITORING AGENCY NAME & ADDRESS (if different from Controlling Office): 77p.	15. SECURITY CLASS. (of this report): Unclassified / 15a. DECLASSIFICATION/DOWNGRADING SCHEDULE

16. DISTRIBUTION STATEMENT (of this Report)

Approved for public release; distribution unlimited.

17. DISTRIBUTION STATEMENT (of the abstract entered in Block 20, if different from Report)

Approved for public release; distribution unlimited.

18. SUPPLEMENTARY NOTES

19. KEY WORDS (Continue on reverse side if necessary and identify by block number)

ultrasonic reflectivity, bounded beam, numerical integration method, longitudinal critical angle, Rayleigh critical angle, ultrasonic absorption

20. ABSTRACT (Continue on reverse side if necessary and identify by block number)

A numerical integration method is developed for calculating the changes in beam profile and amplitude upon reflection of a bounded ultrasonic beam incident on a liquid-solid flat interface at the longitudinal wave critical angle and the Rayleigh angle. No approximations, valid only at the Rayleigh angle, are used, and the method is applicable to all angles of incidence.

DD FORM 1 JAN 73 1473 EDITION OF 1 NOV 65 IS OBSOLETE S/N 0102-014-6601

Unclassified

SECURITY CLASSIFICATION OF THIS PAGE (When Data Entered)

153 620

79 07 30 121

This Technical Report describes work performed by T. D. K. Ngoc for his doctorate in Physics at Georgetown University. The study contained in the Report is part of the Project supported by the Office of Naval Research, Physics Program (Code 421), under Contract N00014-78-C-0584.

The study is concerned with the influence of absorption on the numerical values of the reflectivity of a bounded ultrasonic beam reflected from a liquid-solid interface. Particular attention is given to changes in the beam profile upon reflection at the critical angles. Only approximate values of the beam parameters had been available until now; the numerical integration method described in this Report yields exact values for all angles of incidence.

Walter G. Mayer
Principal Investigator

July 1979.

ABSTRACT

A theoretical and experimental investigation of non-specular ultrasonic reflectivity at a liquid-solid interface is described. The role of attenuation in the formulation of the plane wave reflection coefficient is analyzed. This attenuation-dependent reflection coefficient is used in a numerical integration method which is developed for the calculation of the reflected beam profile. The results are compared with other existing formulations. The reflected profile is calculated by this numerical approach for two specific cases: incidence near the Rayleigh angle for a water-stainless steel interface and incidence near the longitudinal critical angle for a water-Plexiglas interface. In each case, the non-specular reflection effects are investigated as one parameter is varied and the others are kept unchanged. Comparisons are made with results obtained by the Bertoni and Tamir formulation for incidence at the Rayleigh angle. The theoretical predictions are then compared to experimental results obtained by the Schlieren visualization technique.

CHAPTER I

INTRODUCTION

The reflection coefficient derived from the plane wave theory is inadequate in describing the reflection of ultrasonic waves incident from a liquid medium onto a flat liquid-solid interface. In practice, the sound waves are normally generated by a source of finite dimensions and thus cannot be considered as plane waves. From the plane wave theory, it is expected that the reflected sound beam has the same intensity distribution as that of the incident beam at the reflecting interface; or, in other words, it is specularly reflected. However, several interesting phenomena, known as non-specular reflection effects, have been observed in experiments as a result of the boundedness of the incident beam, especially for incidence at the Rayleigh critical angle.

The Raleigh critical angle is a particular angle of incidence at which the incident longitudinal wave is mode-converted into a leaky Rayleigh surface wave. The characteristics of this surface wave are that its magnitude decreases rapidly with distance from the interface, its propagation velocity is less than the shear wave velocity in the solid, and it loses energy through reradiation into the liquid. For a liquid-solid structure, the plane wave theory also predicts the existence of the longitudinal and shear critical angles. The longitudinal critical angle is the angle of incidence beyond which only refraction of shear waves is possible; and the shear critical angle is the lower

limit of the incident angular range that results in total reflection.

The first analytical formulation developed to treat the reflection of a bounded ultrasonic beam for a liquid-solid interface was established by Schoch [1]. Schoch's model predicts a lateral displacement of the reflected beam for all incident angles, which, including the Rayleigh angle, result in total reflection. Nevertheless, his model fails to account for other non-specular reflection features, such as the possible intensity null and the widening of the reflected beam, experimentally observed for incidence at the Rayleigh angle. Another formulation, derived by Bertoni and Tamir [2] to treat non-specular reflectivity specifically for Rayleigh angle incidence, eliminates these discrepancies and explains the basic non-specular reflection phenomena at that critical angle.

In essence, these two formulations are based upon the principle of spectral representation of a bounded beam. Their main difference stems from their different methods of approximating the reflection coefficient. Schoch approximates the reflection coefficient as a product of its magnitude and phase with the former being assumed constant and the latter slowly varying. The expression of the reflection coefficient is a ratio whose numerator and denominator are complex functions of the incident angle and both become zero for incidence at the Rayleigh critical angle. Taking advantage of the existence of a pole-zero pair at the Rayleigh angle, Bertoni and Tamir used a complex Laurent series expansion to simplify the mathematically complicated expression of the reflection coefficient in terms of its pole and zero. It is then evident that the Bertoni and Tamir formulation describes non-specular

reflection phenomena which are caused by the interference of the specularly reflected beam and a trailing field, that is, a widening of the reflected beam. Schoch, on the other hand, explains only a beam displacement resulting from the phase shift generated by the reflection of sound waves at the interface. Because of its incomplete assumptions concerning the reflection coefficient, Schoch's approach has not provided correct results, especially at the critical angles.

The Bertoni and Tamir formulation, although providing predictions qualitatively consistent with experimental observations, has some limitations. It is applicable only at the Rayleigh critical angle and leads to analytical difficulties when extended to non-Gaussian profiles for the incident beam. Nonetheless, its success is one of the reasons why non-specular reflectivity at the Rayleigh angle has been studied extensively. Since the Bertoni and Tamir theory applies only to Rayleigh angle incidence, little is known about the possible non-specular reflection phenomena for bounded beams incident at or near the longitudinal and shear critical angles. Preliminary experimental evidence indicating the existence of non-specular reflectivity similar to that at the Rayleigh angle was reported by Neubauer [3] for Mallory 1000 at the shear critical angle and for Pyrex glass at the longitudinal critical angle. However, there exists no published theoretical analysis of these results.

The difficulties in a theoretical analysis of the possible non-specular reflectivity near the longitudinal and shear critical angles are mainly due to the singular behavior of the reflection coefficient at these angles. The analytical properties of the reflection

coefficient, concerning its complex singularities, together with the contour integration process, involved in the spectral representation of a bounded beam, have been studied extensively by several authors [2,4,5] for the lossless situation. Inclusion of attenuation in the media leads to a more realistic description of the non-specular reflection effects and, at the same time, removes these analytical difficulties as will be shown later.

Attenuation in the media further complicates the physical problem under consideration. Becker and Richardson [4] investigated the influence of absorption on reflectivity to find that the reflection coefficient behaves differently when absorption is taken into account. Total reflection is then not expected at any angle of incidence and the reflection amplitude and phase are shown to significantly deviate from the lossless case. Bertoni and Hou [6] have recently incorporated attenuation into a theoretical investigation of non-specular reflectivity at the Rayleigh angle. Pitts, Plona, and Mayer [5] have extended Bertoni and Tamir's model to a more complicated case of a solid plate immersed in a liquid. In the same analytical framework, Breazeale et al [7] examined the reflected beam profiles observed at large distances from the liquid-solid interface.

This thesis will deal with the problem of non-specular reflectivity in the presence of attenuation covering the complete range of incident angles. The reflected beam profile will be calculated via a numerical integration method for a Gaussian incident beam to facilitate comparison with earlier calculated results. Finally, the theoretically obtained profile will be experimentally verified. A Schlieren

visualization technique is used for the experimental verification.

Chapter II is a presentation of a detailed investigation of the plane wave reflection coefficient for the liquid-solid case. The reflection coefficient plays an important role in determining the reflected beam profile since the bounded incident beam is to be considered as a superposition of an infinite number of plane waves each being reflected in accordance with the plane wave reflection coefficient. The influence of absorption in the non-specular reflectivity problem is considered by explicitly introducing the attenuation parameters into the reflection coefficient. Special emphasis is given to the behavior of the reflection amplitude and phase near the critical angles.

In Chapter III, the existing theoretical methods of treating non-specular reflectivity are discussed in detail. A condensed review of the Schoch and the Bertoni and Tamir formulations is presented in preparation for the introduction of the numerical integration method. The chapter is concluded with a comparative analysis of these formulations.

Chapter IV is devoted to a presentation and discussion of the results of the numerical integration method. It was observed [2] that the reflected beam profile is a strong function of the angle of incidence, the sound frequency, and the beam width. The most significant contribution of the numerical integration method is its ability to describe the reflected profile for all angles of incidence. In addition, when attenuation is included, the frequency dependence of the reflected profile is directly established in this formulation. The reflected beam profile is then calculated for different values of one parameter while keeping the others constant. Although the calculation can be performed

for any angle of incidence, the results given here are limited to angular ranges near the critical angles where non-specular reflectivity is prominent. These results are compared to those obtained by the Bertoni and Tamir method wherever that method is applicable.

Experimental results are presented and analyzed in Chapter V. Due to the broad nature of the non-specular reflectivity problem, the experimental effort is focused only on its major aspects. Variation of the reflected beam profile as a function of the angle of incidence near the Rayleigh and longitudinal critical angles is investigated for water-Plexiglas and water-stainless steel interfaces.

The final chapter contains a summary of the main results, possible extensions of the numerical integration approach, and questions remaining to be answered.

During the course of the theoretical investigation, four computer programs written in the FORTRAN IV language were developed to

(i) Calculate the magnitude and the phase of the plane wave reflection coefficient,

(ii) Search for the locations of the Rayleigh pole-zero pair,

(iii) Determine the reflected profile using Bertoni and Tamir's results, and

(iv) Compute the reflected profile through the numerical integration process.

Representative versions of these programs, which are at times slightly modified to suit certain calculation purposes, are listed for reference in the appendices.

CHAPTER II

PLANE WAVE REFLECTION COEFFICIENT FOR AN ABSORPTIVE LIQUID-SOLID INTERFACE

The plane wave reflection coefficient plays a central part in determining the reflected profile for a bounded incident beam. Understanding its behavior with respect to different angles of incidence provides a useful perception of the non-specular reflectivity problem. This chapter examines the singularities of the complex plane wave reflection coefficient and the variation of its amplitude and phase as functions of the angle of incidence. The first section describes investigations of the analytical properties of the lossless reflection coefficient for various typical liquid-solid combinations. In the second section, various published treatments of attenuation are reviewed and a specific manner of incorporating absorption into the reflection coefficient is presented. With attenuation included, the final section is devoted to a detailed investigation of these aspects near the three critical angles.

A. Lossless Reflection Coefficient for a Liquid-Solid Interface

Consider an infinite longitudinal plane wave with an angular frequency ω, incident from a liquid medium at an angle θ_i, and onto a liquid-solid interface of two isotropic, perfectly elastic infinite half-spaces. The incident wave travels with a velocity v and part of its energy is reflected back into the liquid. The other part is refracted

as two separate waves traveling in the solid with a longitudinal wave velocity v_d and a shear wave velocity v_s, respectively. The coordinate system is chosen such that the x-axis is along the interface and the z-axis normal to it. There is no y variation since the wave is assumed to be infinitely extended in the y direction. The above description is illustrated in Fig. 1. The derivation of the amplitude reflection coefficient for such a liquid-solid interface has been carried out in detail by several authors [1,8,9]. A convenient form of the plane wave reflection coefficient for the lossless case is given [9] by

$$R(k_x) = \frac{(k_s^2 - 2k_x^2)^2 + 4k_x^2\kappa_s\kappa_d - \rho k_s^4\kappa_d/\kappa}{(k_s^2 - 2k_x^2)^2 + 4k_x^2\kappa_s\kappa_d + \rho k_s^4\kappa_d/\kappa} , \tag{1}$$

where

ρ = liquid density/solid density,

$k = \omega/v$,

$k_d = \omega/v_d$,

$k_s = \omega/v_s$,

$k_x = k\sin\theta_i$,

$\kappa = (k^2 - k_x^2)^{\frac{1}{2}}$,

$\kappa_d = (k_d^2 - k_x^2)^{\frac{1}{2}}$,

$\kappa_s = (k_s^2 - k_x^2)^{\frac{1}{2}}$.

The function $R(k_x)$ is complex due to the existence of several square-root terms in (1). In general, the analytical behavior of $R(k_x)$ is functionally determined by its singularities in the complex k_x-plane and hence should be studied first of all by considering these singularities. For the lossless case, it is well known that there often exist

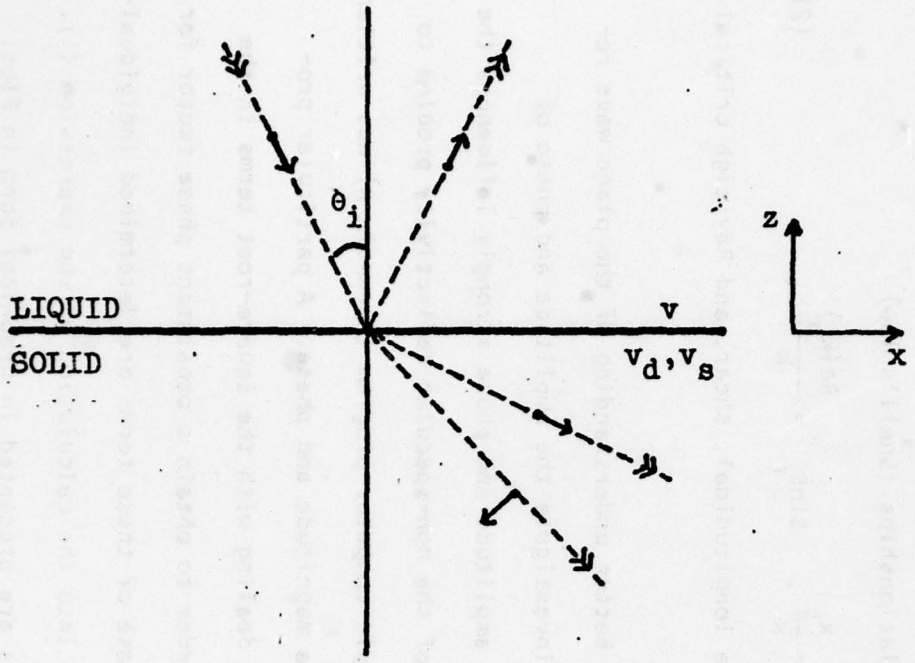

Figure 1. Reflection and refraction of sound at a liquid-solid interface. The directions of propagation are shown with double arrows and the directions of the particle displacement with single arrows.

three pairs of branch points on the real axis located at $\pm k_d$, $\pm k_s$, and $\pm k$ and a pole-zero pair k_p-k_o positioned slightly off the real axis as shown for a typical liquid-solid interface in Fig. 2. Under the boundary conditions associated with the lossless case, it can be shown that $k_o = k_p^*$. Physically, these singular points are related to the critical angles via the following relationships (Snell's law)

$$\text{Sin}\theta_d = \frac{k_d}{k} \; ; \quad \text{Sin}\theta_s = \frac{k_s}{k} \; ; \quad \text{Sin}\theta_r = \frac{\text{Re}(k_p)}{k} \; , \tag{2}$$

where θ_d, θ_s, and θ_r are the longitudinal, shear, and Rayleigh critical angles, respectively.

Another way to gain a better understanding of the plane wave reflection coefficient is to investigate the amplitude and phase of $R(k_x)$. The behavior of the amplitude and phase strongly influences the reflection characteristics of the non-specular reflectivity problem to be considered later. A simple computer program (Appendix A) was written to numerically calculate the magnitude and phase. A particular programming problem appears in dealing with the square-root terms in the expression for $R(k_x)$. In order to obtain a consistent phase factor for $R(k_x)$, the magnitude and phase of these terms are determined individually before they are inserted into the calculation of the expression (1).

The calculated results are presented in graphical form in Figs. 3 and 4 for two interfaces: water-stainless steel and water-Plexiglas. The values of sound velocities and density ratios used for these materials are given in Table 1. The curves for the water-stainless steel case, in general, represent a typical water-metal combination. Total reflection at the longitudinal critical angle and beyond the shear

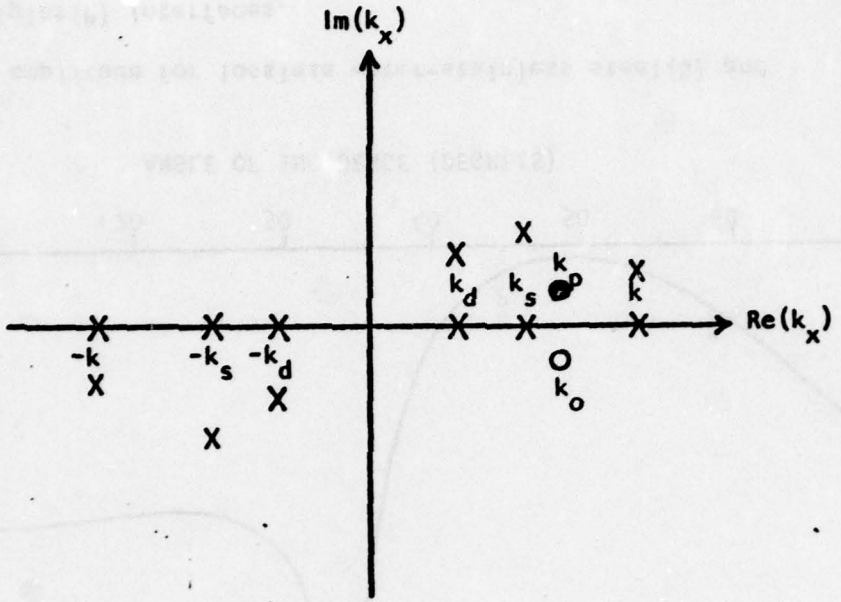

Figure 2. Singularities of $R(k_x)$ in the complex k_x-plane. Branch points are indicated by crosses, pole by black dot and zero by white dot. For a typical absorptive $R(k_x)$, the possible branch points are removed off the real axis as shown.

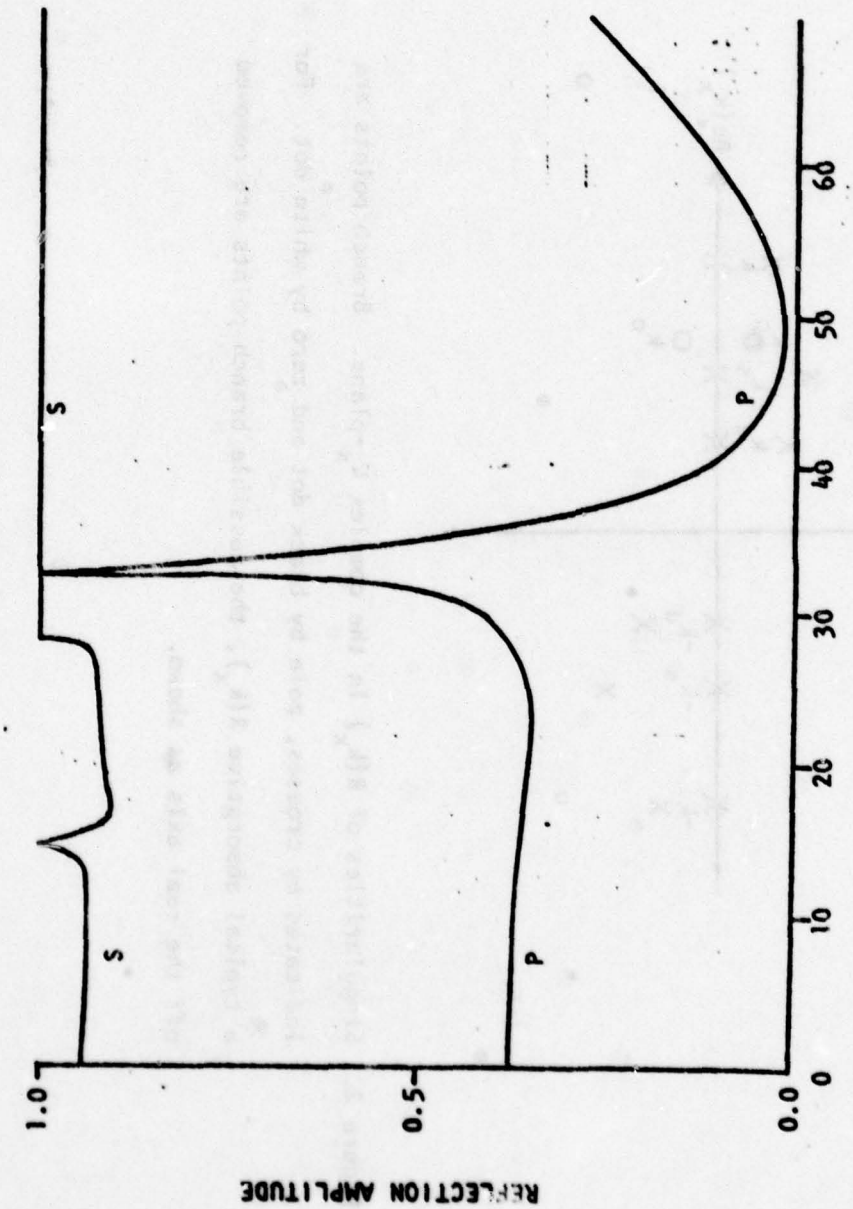

Figure 3. Reflection amplitude for lossless water-stainless steel(S) and water-Plexiglas(P) interfaces.

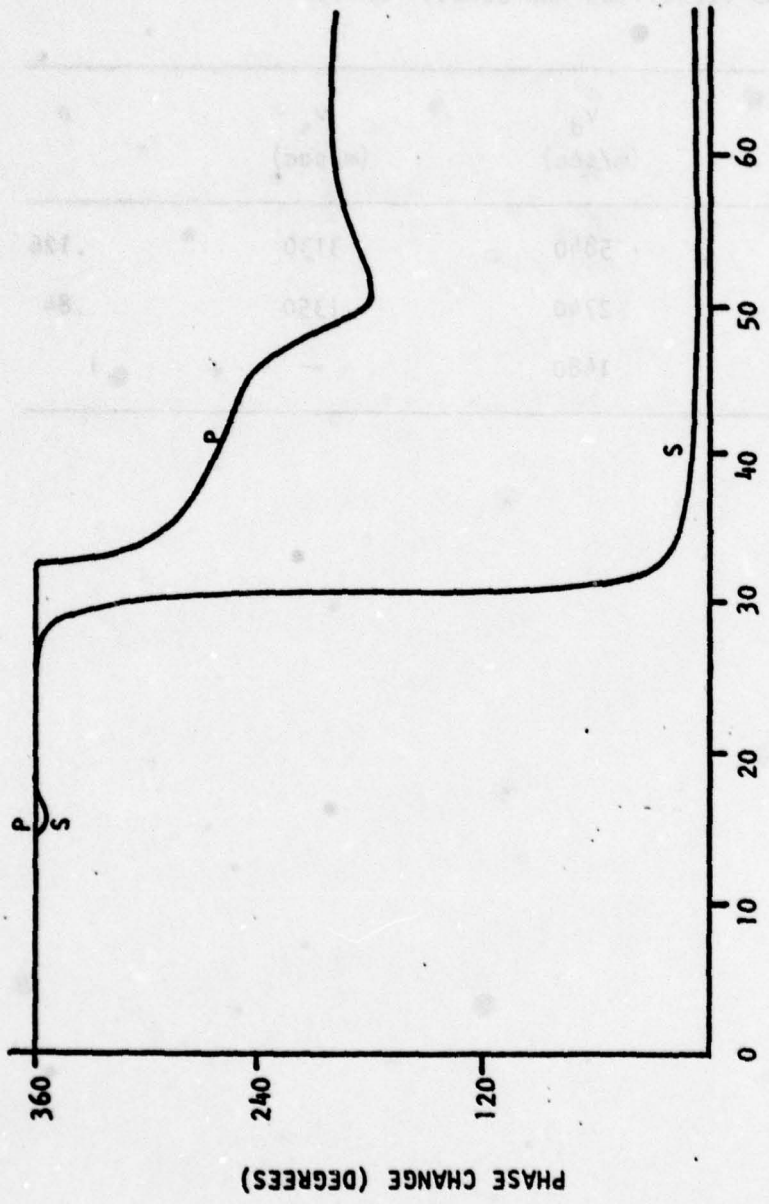

Figure 4. Phase change upon reflection for lossless water-stainless steel (S) and water-Plexiglas (P) interfaces.

TABLE 1

SOUND VELOCITIES AND DENSITY RATIOS

Materials	v_d (m/sec)	v_s (m/sec)	ρ
Stainless steel	5840	3130	.126
Plexiglas	2740	1350	.84
Water	1480	--	1

critical angle occurs as is usually predicted for lossless media. The phase curve exhibits a small dip at the longitudinal critical angle and an almost 360° phase shift at the Rayleigh angle. Special variation one might expect at the shear critical angle is not apparent due to its close proximity with respect to the Rayleigh critical angle.

Because the shear wave velocity of Plexiglas is less than the sound velocity in water, the magnitude and phase of the reflection coefficient for the water-Plexiglas interface behave in a different manner compared with most other liquid-solid combinations. There exist only two pairs of branch points corresponding to the longitudinal critical angle and the angle of glancing incidence, $\theta_i = 90^\circ$. The Rayleigh pole-zero pair is suppressed and no Rayleigh surface wave can be generated in this case. The magnitude of the reflection coefficient has a very sharp peak at the longitudinal critical angle and decreases to almost zero before gradually returning to total reflection at glancing incidence. Starting from the longitudinal critical angle, the phase drops slowly from 360° to 180° at $\theta_i = 90^\circ$. The manner in which the phase decreases in this range is found to depend mainly on the different values of the shear wave velocity used for different Plexiglas samples. It should be noted that the slopes of the magnitude and phase curves exhibit a discontinuity whenever there exist a pair of branch points.

B. Incorporation of Absorption into Reflection Coefficient

It has been realized [2,4,6] that attenuation in materials would affect the non-specular reflection phenomena at the Rayleigh critical angle. The current procedure to account for attenuation, which has

proved to be satisfactory, is to define a loss parameter from the traditional attenuation constant and to incorporate it in the wave number, which then becomes complex. Denoting these loss parameters as a, a_d and a_s for the sound waves in the liquid, the longitudinal and shear waves in the solid, respectively, one can write the complex wave numbers as

$$\begin{aligned} k &= (\omega/v)\ (1 + ia/2\pi)\ , \\ k_d &= (\omega/v_d)\ (1 + ia_d/2\pi)\ , \\ k_s &= (\omega/v_s)\ (1 + ia_s/2\pi). \end{aligned} \tag{3}$$

The loss parameters can then be identified as attenuation per wavelength in nepers and are related, for example, to the attenuation constant α of the liquid medium by

$$a = 2\pi \frac{\alpha v}{\omega} = \frac{\alpha v}{f} = \alpha \lambda\ , \tag{4}$$

where f and λ are the sound frequency and wavelength.

In investigating the influence of attenuation on the reflection coefficient, earlier authors [2,4] observed that $R(k_x)$ depends on the loss parameters, or the product $\alpha\lambda$, rather than on attenuation or frequency alone. Accordingly, they made use of different values of the loss parameters without considering separately either frequency or attenuation. However, some results obtained in such calculations are of little practical use since attenuation in most materials is a nonlinear function of frequency. Thus one does not have the freedom to separately select the values of frequency and attenuation to arrive at

a given set of loss parameters. In practice, it is more desirable to be able to treat frequency as an independent quantity. This can be achieved provided the functional relationship between attenuation and frequency can be determined.

Another aspect concerning the method of introducing attenuation into the reflection coefficient by the same authors [2,4] should also be mentioned here. In dealing with reflection phenomena taking place at the Rayleigh critical angle, Bertoni and Tamir [2] assumed $a_d = a_s$ because the pole-zero pair locations did not vary significantly with a_d. Becker and Richardson [4], on the other hand, calculated the magnitude and phase of $R(k_x)$ for a given set of separate loss parameters, assuming a constant longitudinal-to-shear attenuation constant ratio. Finally, they all neglected attenuation in the liquid medium.

The results to be obtained for the case of absorptive media in this work are not subject to the above-mentioned limitations. Frequency is used as an independent parameter and therefore leads to definite frequency-dependent values of the loss parameters. The loss parameters are determined from attenuation constants experimentally measured for various frequencies as described in Chapter V. This procedure was selected in order to allow comparison of calculated results with experimental measurements of non-specular reflectivity.

C. Absorptive Reflection Coefficient near Critical Angles

After incorporating attenuation into the reflection coefficient, one can now determine the analytical properties of the absorptive $R(k_x)$. In the following, calculations are again presented for water-stainless steel and water-Plexiglas interfaces. The values to be used for the

loss parameters are tabulated in Table 2. The attenuation constants were measured for the samples which were used in experiments described in Chapter V. As will be seen below, the introduction of attenuation leads to two developments: the positions of the singularities are displaced from those of the lossless case; and the magnitude and phase curves are different from the lossless ones, especially near the critical angles. At these critical angles, the lossless curves (Figs. 3 and 4) are not smooth but the absorptive ones become smoothly-varying.

The first development is illustrated by tracing the loci of the singular points in the complex k_x-plane. The branch points and their associated branch cuts are displaced vertically off the real axis; this displacement increases with increasing frequency-dependent attenuation, Fig. 2. Accordingly, the pole and zero positions also change with the frequency. Their new locations are determined by a computer program developed to search for the zeroes of the numerator and denominator of the absorptive $R(k_x)$ utilizing the Newton-Raphson algorithm (Appendix B). Figure 5 depicts such loci of the absorptive pole-zero pair as the frequency varies up to 40 MHz for a water-stainless steel interface. It is noted that in the absorptive case the angle of incidence at which the leaky Rayleigh mode is generated depends on the sound frequency since the real part of k_p now assumes a slightly different value from the lossless case.

The other development is the change in the shape of the magnitude and phase curves. Again the magnitude and phase of $R(k_x)$, which now contains the loss parameters, are calculated for the water-Plexiglas and water-stainless steel combinations. In the water-Plexiglas case,

TABLE 2

ATTENUATION DATA

f (MHz)	α_d (Neper/m)	α_s (Neper/m)	a_d	a_s
Stainless Steel				
1	.027	.025	.00004	.000037
2	.229	.330	.00017	.00024
3	.795	1.49	.00039	.00073
6	6.68	19.6	.00165	.00483
10	32.1	131	.00474	.0194
15	111	590	.0111	.0583
20	269	1720	.0199	.1273
25	535	3943	.0317	.2333
30	936	7764	.0462	.3830
35	1503	13770	.0635	.5823
40	2265	22620	.0838	.8369
Plexiglas				
1	7	.0104	7.2	.0107
2	36.6	.0271	67.0	.0496
3	88.4	.0436	247	.1219
6	416	.1027	2298	.5670
Water				
			.00026*	

(*) The attenuation constant for water is assumed to be a linear function of frequency and therefore its loss parameter is considered to be a constant for the frequency range used.

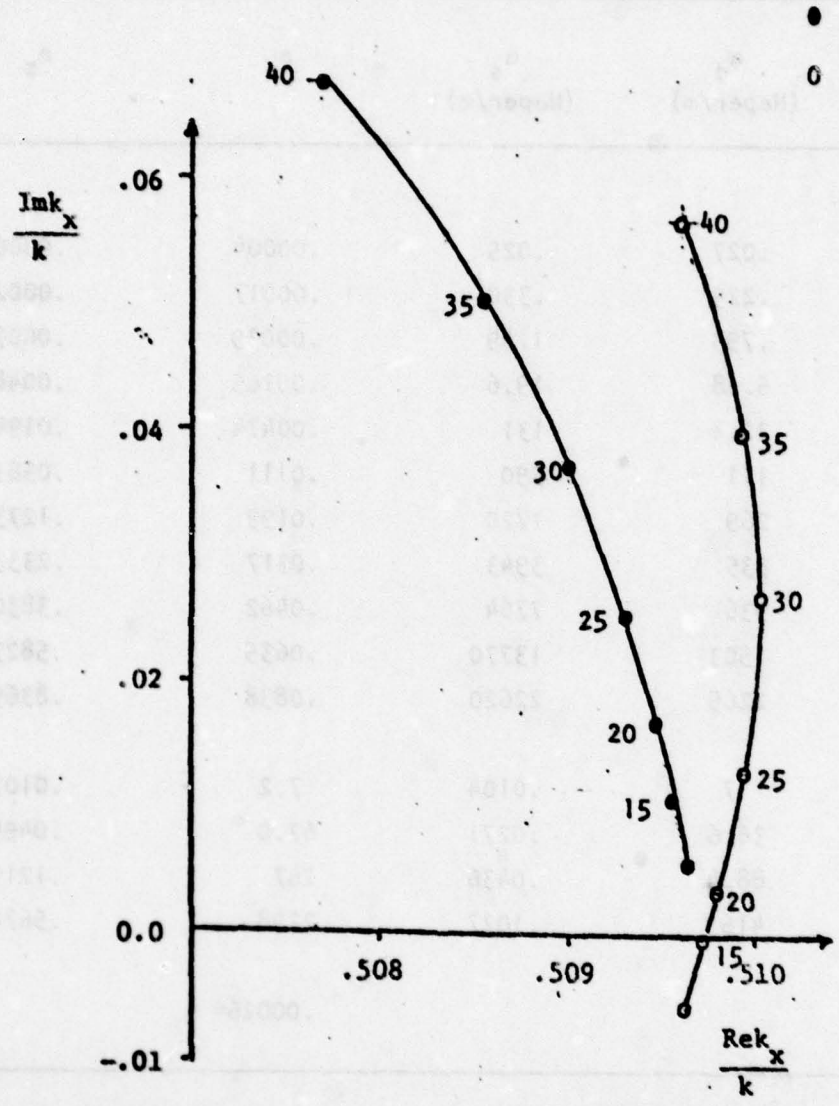

Figure 5. Pole and zero locations of the absorptive $R(k_x)$ for different loss parameters in the frequency range up to 40 MHz for a water-stainless steel interface. The numbers beside the poles or zeroes indicate the associated frequency in MHz starting from the lossless locations.

the difference between the lossless and absorptive $R(k_x)$ is most significant near the longitudinal critical angle. Figure 6 shows the magnitude and phase as functions of the incident angle in the vicinity of the longitudinal critical angle. It is seen that the magnitude of the reflection maximum drops considerably with increasing frequency in the magnitude curve, and that the non-smoothly varying behavior associated with the longitudinal critical angle disappears in both magnitude and phase curves. It is also observed that the reflection amplitude is maximum at slightly different angles of incidence. For the water-stainless steel interface, the change in these curves is most noticeable in the angular range containing both the shear and Rayleigh critical angles. Figure 7 shows the familiar "least reflection frequency" effect, which has been reported by other authors [2,4], arising out of the inclusion of attenuation into the lossless reflection coefficient. This effect is characterized by the appearance of a sharp minimum in the reflection magnitude curve exactly at the Rayleigh critical angle. In Fig. 7, this sharp dip is seen to vary with the frequency and to reach the lowest value at about 15 MHz. It can be shown that the frequency at which the reflection amplitude is zero at the Rayleigh critical angle corresponds to the point where the locus of the zero of the absorptive $R(k_x)$ cuts the real axis in the complex k_x-plane. It should be pointed out that it is no longer tenable to maintain the long-standing association of the longitudinal critical angle, defined by Snell's law, with a reflection maximum as a result of the inclusion of attenuation. It is also true that the shear critical angle of an absorptive liquid-solid interface loses its "critical" character primarily because it is too

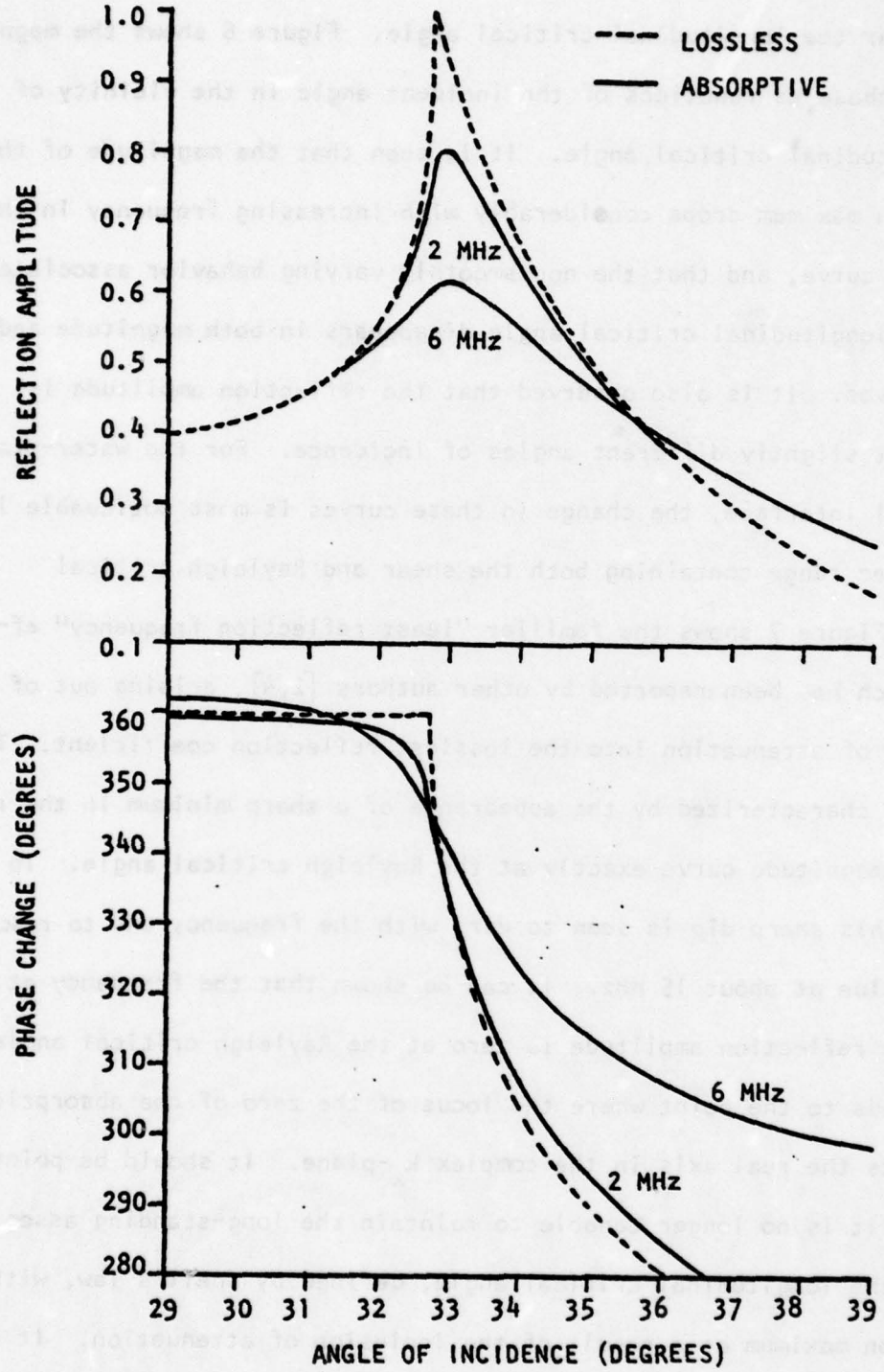

Figure 6. Magnitude and phase of the absorptive $R(k_x)$ near the longitudinal critical angle for a water-Plexiglas interface.

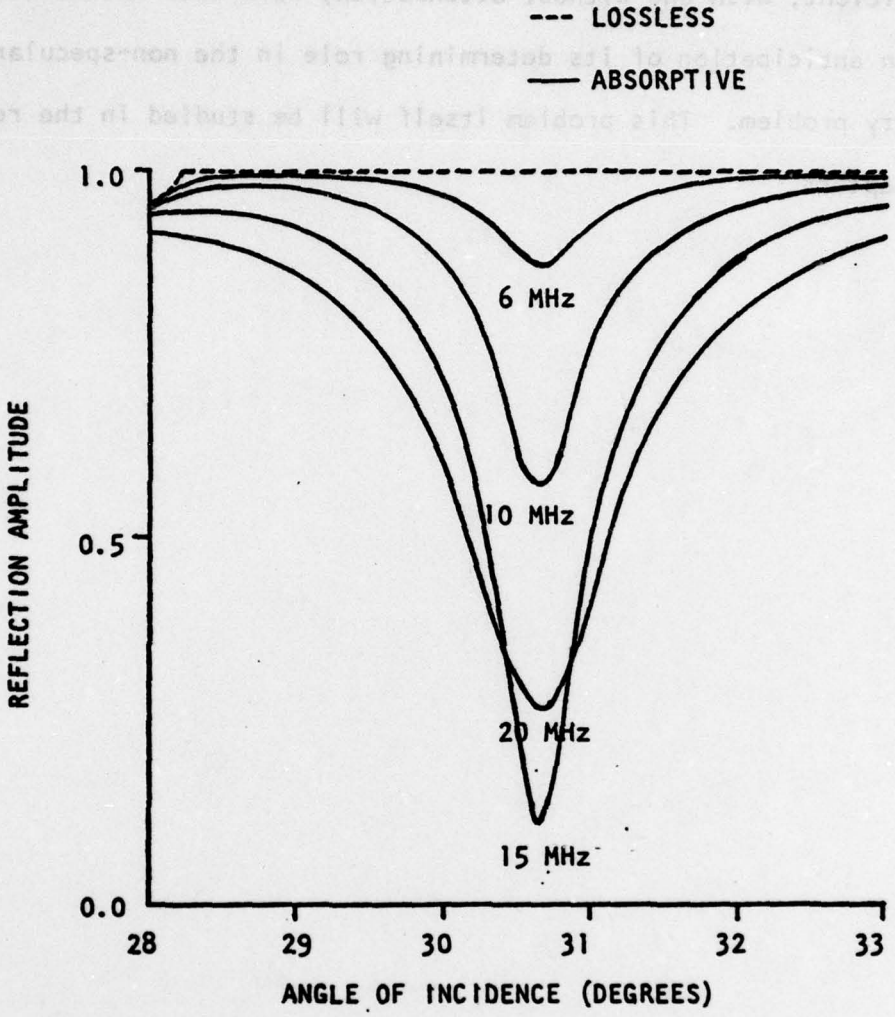

Figure 7. Magnitude of the absorptive $R(k_x)$ near the Rayleigh critical angle for a water-stainless steel interface.

close to the Rayleigh critical angle.

In this chapter, the essential features of the plane wave reflection coefficient, with and without attenuation, have been extensively examined in anticipation of its determining role in the non-specular reflectivity problem. This problem itself will be studied in the remaining chapters.

CHAPTER III

THEORETICAL FORMULATIONS OF NON-SPECULAR REFLECTIVITY

This chapter presents different theoretical formulations designed to explain the experimentally observed non-specular reflection phenomena which arise in practice when a bounded ultrasonic beam is incident onto an interface. All formulations to be discussed here are constructed from the principle of spectral representation of a finite beam but, in general, their success originates largely in their particular method of treating the complex plane wave reflection coefficient which plays a central part in these formulations. In the following, the common method of representing a bounded beam is briefly reviewed before the various formulations are discussed together with methods of treating the reflection coefficient. the chapter is to be concluded with a critical evaluation of these formulations.

A. Spectral Representation of a Bounded Ultrasonic Beam

Consider an incident beam of which the cross-section in the (x,z) plane is bounded and which is uniform along the y-direction, that is, there is no spatial y dependence. With respect to the liquid-solid interface, the coordinate system is chosen as shown in Fig. 8, where the incident beam is taken to be incident at an angle θ_i and its profile is contained by an effective width 2w, projected onto the interface as $2w_o$ given by $w_o = w \sec \theta_i$.

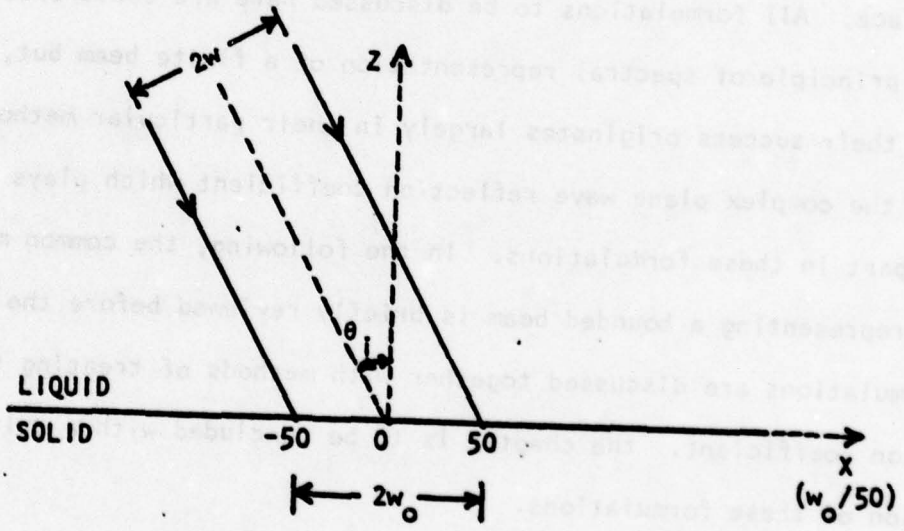

Figure 8. A schematic diagram of a bounded ultrasonic beam incident on a liquid-solid interface.

It is shown [8] by using Fourier analysis that the incident field of a beam can be uniquely determined at any point (x,z) if the field distribution is known in any plane. Describing the acoustic field in terms of the z-component of the particle displacement, the incident field can be expressed as a sum of infinite plane waves by means of the Fourier integral-transform pair

$$U_{inc}(x,z) = (2\pi)^{-1} \int_{-\infty}^{+\infty} V(k_x) \exp[i(k_x x + k_z z)] \, dk_x \tag{5}$$

$$V(k_x) = \int_{-\infty}^{+\infty} U_{inc}(x,0) \exp(-ik_x x) \, dx \, , \tag{6}$$

where the time dependence exp (-iωt) is suppressed, k_x is the x-component of the wavenumber vector, $V(k_x)$ is interpreted as the amplitude of each of the constituent infinite plane waves, and the z-component of the wavenumber vector k_z is defined by $k_z = (k^2 - k_x^2)^{\frac{1}{2}}$.

It has been assumed that the effective beam width is 2w and the beam strikes the interface over a width $2w_o$. For a well-defined beam, neglecting beam spreading, one should expect contributions to the integral in (5) only from those infinite plane waves which are defined by

$$k_i - \pi/w_o \leq k_x \leq k_i + \pi/w_o \tag{7}$$

and the limits of integration in (6) should be

$$-w_o \leq x \leq +w_o \, , \tag{8a}$$

where

$$k_i = |k| \sin\theta_i = (\omega/v) \sin\theta_i = (2\pi/\lambda) \sin\theta_i \ . \qquad (8b)$$

In view of the fact that the integral in (5) is carried out along the real axis and that k_x is varied in a narrow range around k_i, it can be seen from (8b) that the above mathematical representation of a bounded beam entails two possible physical interpretations: either the bounded beam is composed of an infinite number of plane waves having the same wavelength but incident at different angles; or the beam consists of parallel plane wave rays with a small perturbation in wavelength due to the non-uniformity of the sound frequency. In practice, one may expect both physical situations when the experimental procedure of generating the sound beam is brought into consideration. In this and subsequent chapters, k_x is treated as an ultimate independent variable without taking into account the physical reasons behind its variation.

Extending the spectral representation of a bounded beam to the reflected sound beam, one can also represent the reflected field as a superposition of infinite plane waves [2]. The reflected beam profile can now be determined by integrating over individual plane waves whose magnitude is multiplied by the reflection coefficient. Thus the z-component of the reflected field is written as

$$U_{ref}(x,z) = (2\pi)^{-1} \int_{-\infty}^{+\infty} R(k_x)V(k_x)\exp\left[i(k_x x + k_z z)\right] dk_x \ , \qquad (9)$$

where $R(k_x)$ is given by (1).

At the interface, $z = 0$, (9) reduces to

$$U_{ref}(x,0) = (2\pi)^{-1} \int_{-\infty}^{+\infty} R(k_x)V(k_x)\exp(ik_x x)\, dk_x \quad . \tag{10}$$

According to (9), the reflected beam profile is constructed by the interference of an infinite number of reflected plane waves, which have an amplitude $V(k_x)R(k_x)$ and undergo a phase shift introduced by $R(k_x)$ upon reflection. As a result of this very method of constructing the reflected field distribution, deviation from the incident beam profile is expected to be substantial where either the magnitude or the phase of $R(k_x)$ changes appreciably. This is the cause for the earlier anticipation that non-specular reflection phenomena would be most visible near certain critical angles.

Due to the mathematically complicated form of $R(k_x)$ in (9), the integral in most of the cases cannot be evaluated in closed form. In order to overcome this difficulty, several authors have developed various analytical methods of simplifying the integrand in order to evaluate this integral. The remaining sections of this chapter are intended to review these formulations and to introduce a numerical integration method together with a comparative analysis of their relative usefulness.

B. Schoch Treatment of Reflected Beam Profile

On the basis of the spectral representation principle, Schoch [1] sought a theoretical explanation for the non-specular reflection phenomena. His formulation is intended to investigate the reflected beam profile in the neighborhood of those incident angles that lead to total reflection. Since this formulation is constructed with the lossless reflection coefficient in the integrand of (9), the amplitude of $R(k_x)$ is assumed to be constant for the considered angles of incidence and

its phase is assumed to vary slowly in such circumstances. Under these assumed conditions, the plane wave reflection coefficient is simplified by a first-order Taylor series expansion to become [8]

$$R(k_x) \cong |R(k_i)| \exp\left[i(k_x - k_i)\phi'(k_i)\right] , \tag{11}$$

where ϕ' is the first derivative of the phase $\phi(k_x)$ of $R(k_x)$ and both the magnitude and ϕ' are evaluated at k_i. Substituting (11) into (9), one obtains

$$U_{ref}(x,z) \cong (2\pi)^{-1}|R(k_i)|\exp\left[-ik_i\phi'(k_i)\right] \cdot \int_{-\infty}^{+\infty} V(k_x) \exp\left\{ ik_x[x + \phi'(k_i)] + ik_z z \right\} dk_x . \tag{12}$$

Comparing (12) and (5), it is found that

$$U_{ref}(x,z) \cong |R(k_i)|\exp\left[-ik_i\phi'(k_i)\right] U_{inc}\left[x + \phi'(k_i)\right] . \tag{13}$$

The expression (13) indicates that the beam is displaced along the interface by a distance

$$\Delta_S = -\phi'(k_i) . \tag{14}$$

For the reflected beam profile, Schoch's derivation thus predicts a lateral shift that depends solely on the first derivative of the relative phase function of the plane wave reflection coefficient. Schoch's result has been shown in many cases to be incompatible with experimental observations near the critical angles. Its failure can be traced back to the facts that (i) his derivation is based on simplistic assumptions

implied in the behavior of the lossless reflection coefficient, and (ii) it does not consider the existence of singularities of $R(k_x)$, that is, the singular behavior of $R(k_x)$ near the critical angles. In retrospect, Schoch's analysis, in its simple form, has shown that there always exists, although insignificant, a certain amount of non-specular reflectivity in the form of a beam displacement for those angles of incidence at which $R(k_x)$ satisfies the assumed conditions on magnitude and phase.

C. Bertoni and Tamir Formulation for Incidence at the Rayleigh Critical Angle

In another way to overcome the analytical difficulty caused by the complicated form of $R(k_x)$, Bertoni and Tamir [2], taking advantage of the existence of the pole-zero pair associated with the Rayleigh critical angle in order to simplify $R(k_x)$, were able to carry out the integration in (9) in closed form. The reflection coefficient is expanded in terms of a Laurent series with only the most significant term being retained, giving rise to

$$R(k_x) = \frac{k_x - k_o}{k_x - k_p} \quad . \tag{15}$$

A convenient form of the incident beam is a Gaussian distribution of half-width w. Hence the incident sound field can be characterized by

$$U_{inc}(x,0) = \exp\left[-(x/w_o)^2 + ik_i x\right] \quad , \tag{16}$$

which is normalized to unity. To determine the reflected beam profile, one needs to find the Fourier transform of $U_{inc}(x,0)$ in the k_x-plane. Inserting (16) into (6), one obtains

$$V(k_x) = \pi^{\frac{1}{2}} w_o \exp\left[-(k_x - k_i)^2 (w_o/2)^2\right] . \tag{17}$$

Substituting (15) and (17) into (10), the reflected field distribution at z = 0 is found to be [2]

$$U_{ref}(x,0) = \frac{k_i - k_o}{k_i - k_p} U_{inc}(x,0) \tag{18}$$

$$+ \frac{k_p - k_o}{k_p - k_i}\left[1 + \frac{i\pi^{\frac{1}{2}}}{2} w_o (k_p - k_i) \exp(\gamma^2) \operatorname{erfc}(\gamma)\right] U_{inc}(x,0),$$

where erfc(γ) is the complementary error function of argument

$$\gamma = \frac{w_o \operatorname{Im}(k_p)}{2} - \frac{x}{w_o} + i\,\frac{[k_i - \operatorname{Re}(k_p)] w_o}{2} . \tag{19}$$

For incidence at the Rayleigh angle,

$$k_i = \operatorname{Re}(k_p)$$

and

$$\gamma = \frac{w_o \operatorname{Im}(k_p)}{2} - \frac{x}{w_o} ,$$

the incident and reflected beam intensity can be described by

$$|U_{inc}(x,0)|^2 = \exp\left[-2(x/w_o)^2\right] \tag{20}$$

and

$$|U_{ref}(x,0)|^2 = |R_1 + R_2R_3|^2 \, |U_{inc}(x,0)|^2 \quad , \tag{21}$$

where

$$R_1 = \frac{k_o - Re(k_p)}{Im(k_p)} \quad ,$$

$$R_2 = \frac{k_p - k_o}{Im(k_p)} \quad ,$$

$$R_3 = 1 - \frac{\pi^{\frac{1}{2}} w_o Im(k_p)}{2} \exp(\gamma^2) \, erfc(\gamma) \quad .$$

With the above formulation, Bertoni and Tamir have provided a satisfactory model in describing the essential features of the non-specular reflection phenomena for incidence at the Rayleigh angle. Bertoni and Tamir's model demonstrates that the reflected beam profile exhibits a lateral shift, an intensity null within the reflected beam, and a weakening trailing field as had been experimentally observed [3]. A more accurate quantitative description can be obtained by this model if attenuation in the media is included in the formulation. In the next chapter, some reflected profiles are determined numerically from Bertoni and Tamir's results, including attenuation, for comparison with others. The computer program written for this purpose is illustrated in Appendix C.

By considering separately the two terms in (18), Bertoni and Tamir have demonstrated that the resulting reflected profile was constructed from the interference of the specularly reflected field and the field of

leaky Rayleigh waves. This interpretation is quite adequate for the particular case of non-specular reflectivity at the Rayleigh angle, but is inappropriate to explain the same phenomena at other angles of incidence. This also suggests some limitations of the Bertoni and Tamir formulation: it cannot be used to solve the non-specular reflectivity problem at incident angles other than the Rayleigh angle, and it is not applicable to non-Gaussian incident profiles in general.

D. Numerical Integration Method of Determining Reflected Beam Profile for All Incident Angles

Due to the limitations and restrictions of the Schoch and the Bertoni and Tamir models, another method is needed to investigate the non-specular phenomena at all angles of incidence. Using the spectral representation approach for a bounded beam, a numerical integration computer program (Appendix D) is developed to determine the reflected beam profile given by the integral expressed in (10). The program is built on the basis of the Simpson's integration algorithm applied to complex variables. The integrand is rewritten in terms of dimensionless normalized variables to improve accuracy and to facilitate the input of physical quantities.

First, the wavenumber components are transformed into dimensionless quantities through the following new variables

$$A_x = (v/\omega)\, k_x ,$$

$$A = 1 + ia/2\pi ,$$

$$A_d = (v/v_d)\,(1 + ia_d/2\pi) ,$$

$$A_s = (v/v_s)\,(1 + ia_s/2\pi) ,$$

$$A_i = \sin\theta_i .$$

The square-root terms are redefined accordingly as

$$B = (A^2 - A_x^2)^{\frac{1}{2}} ,$$

$$B_d = (A_d^2 - A_x^2)^{\frac{1}{2}} ,$$

$$B_s = (A_s^2 - A_x^2)^{\frac{1}{2}} .$$

Then the plane wave reflection coefficient given by (1) can be rewritten as

$$R(A_x) = \frac{(2A_x^2 - A_s^2)^2 + 4B_dB_sA_x^2 - \rho A_s^4 B_d/B}{(2A_x^2 - A_s^2)^2 + 4B_dB_sA_x^2 + \rho A_s^4 B_d/B} . \qquad (22)$$

In order to allow comparison later with results obtained by the Bertoni and Tamir formulation, the incident profile used is chosen to be Gaussian and normalized with respect to unity as given in (16). If W denotes the projected half beam width measured in terms of the sound wavelength, i.e. $W = (w_o/\lambda)$, and X the position in units of w_o, i.e. $X = (x/w_o)$, then (10) becomes

$$U_{ref}(X) = (2\pi)^{+\frac{1}{2}} \int_{A_i - W_k}^{A_i + W_k} R(A_x)\, V(A_x)\, E(X,A_x)\, dA_x , \qquad (23)$$

where

$$V(A_x) = W \exp\left[-(\pi W)^2 (A_x - A_i)^2\right] ,$$

$$E(X,A_x) = \exp(i2\pi W A_x X) ,$$

and

$$W_k = 1/2W .$$

The program is constructed to calculate the reflected beam profile in the form of (23) derived from a normalized Gaussian incident profile. A standard accuracy check is performed on the iterative integration process and it is found that an optimized accuracy up to 10^{-8} can be attained when the number of intervals reaches 60. All the calculated results shown in the following chapters are done under these conditions.

E. Comparative Evaluation of Existing Formulations

In this section, a brief summary is given of the procedures used in the past to determine the reflected beam profile. This is presented below so that the relative advantages and disadvantages of the existing methods can be assessed.

Under fairly strict assumptions, which are applicable only to non-critical angular ranges that insure an analytical and slowly-varying behavior for the lossless $R(k_x)$, Schoch's simple derivation consists of an approximation of the term $R(k_x)$. This leads to a prediction of a beam displacement without the need to carry out the actual integration.

In order to arrive at the reflected beam profile via the Bertoni and Tamir formulation, the following steps must be taken: (i) For a liquid-solid combination, their physical properties and the sound frequency are defined; (ii) The Rayleigh pole and zero need to be located; (iii) Since the pole and zero locations change with frequency when the attenuation in materials is accounted for, their loci as functions of the frequency-dependent attenuation in the complex k_x-plane must be found if a more accurate reflected profile is desired; (iv) And finally the pole-zero locations are inserted into the closed form solution given

by (21) to obtain the reflected beam profile at the Rayleigh critical angle.

The numerical integration formulation proceeds in a more direct manner without going through the mode-identifying step required by the Bertoni and Tamir formulation. It consists of: (i) For a given liquid-solid interface, the sound velocities, density ratio and the frequency together with its associated attenuation parameters are determined; (ii) These values are then considered as inputs to a computer program built on the basis of the Simpson's integration algorithm providing an accurate profile of the reflected beam.

It is obvious that the contribution of the Schoch formulation to the theoretical investigation of the non-specular reflection phenomena is the most limited. It fails to provide a complete physical picture for the problem near the critical angles. However, it should be realized that Schoch's result is adequate for describing non-specular reflectivity at non-critical angles of incidence.

In comparing the other two formulations, one sees several advantages of the numerical integration approach over the Bertoni and Tamir analysis: First, the numerical integration method is applicable for all angles of incidence with equal ease and accuracy and thus can present a continuously changing profile of the reflected beam as a function of the incident angles; Second, one does not need to go through the time-consuming process of identifying the Rayleigh mode in the case of investigating the non-specular reflectivity effects near the Rayleigh angle; Third, the same approach can be readily extended to study more subtle aspects of the problem, such as the beam spreading effect, non-Gaussian

incident profiles, and the internal structure of the bounded beam; And finally, its accuracy is sufficient for all practical purposes and can be improved with better possible programming techniques unlike the other formulations where inaccuracy is implicitly built in by various approximations and assumptions.

In conclusion, it should be pointed out, regarding the Bertoni and Tamir formulation, that thanks to its ingenious utilization of the Rayleigh pole-zero pair it is able to present the non-specular reflection phenomena at theRayleigh angle from another useful viewpoint: an interaction of the leaky Rayleigh field and the specularly reflected beam, in addition to the process of interference between infinite plane waves as implied within the spectral representation framework.

CHAPTER IV

REFLECTED BEAM PROFILE CALCULATED BY NUMERICAL INTEGRATION METHOD

The numerical integration method and other theoretical formulations dealing with the non-specular reflectivity effects were presented and evaluated in the previous chapter. The numerical integration method was seen to possess several advantages over the often used formulation developed by Bertoni and Tamir. In this chapter, these advantages are demonstrated through the calculated results obtained by the numerical integration method for various ranges of the incident angle, some of which are made possible only by this numerical approach. The principal parameters affecting the reflected beam profile, in general, are the sound frequency, the beam width, and the angle of incidence. Since the reflected profile is found to have distinct patterns for different ranges of incident angles, the non-specular reflection phenomena are to be investigated separately for the two most significant ranges near the Rayleigh and longitudinal critical angles. The shear critical angle is considered as part of the Rayleigh angular range. In each angular range, the reflected beam profile is determined as one parameter is varied while keeping the others unchanged. In this manner, one can clearly discern the influence exerted on the profile by the beam width and the sound frequency through attenuation in materials. In particular, for the case of incidence at the Rayleigh angle, reflected profiles

calculated from the Bertoni and Tamir formulation are compared to those obtained by the numerical integration method.

A. Reflected Profile for Incidence near Rayleigh Critical Angle

In this section, the reflected profile is to be determined for different angles of incidence near the Rayleigh critical angle by both methods, numerical integration and the Bertoni and Tamir method. Since the Bertoni and Tamir method is an approximate formulation providing accurate results only for the Rayleigh angle, it is used only at that angle while the numerical integration approach is applied for all angles of interest. The profiles produced from the same parametric inputs, shown in Tables 1 and 2, by the two methods are compared wherever possible. The liquid-solid combination chosen is water-stainless steel which is expected to exhibit those non-specular reflectivity effects near the Rayleigh angle, which are typical for many liquid-metal interfaces. Similarly, commonly arising values of the sound frequency and the beam width are used in these calculations.

1. Variation of Beam Profile with Beam Width

A change in the beam width is expected to result in a change in the bounded beam internal structure, which is related to a change in the reflected beam profile via the different functional behavior of $V(A_x)$ and $E(A_x)$ in the integration process expressed by (23). It is realized that a good understanding of these interrelationships would provide a significant insight into the problem of constructing a bounded beam. This represents another major task beyond the scope of the work undertaken at present. Below one is concerned with the direct dependence of the reflected beam profile on the beam width itself.

The reflected beam profile is calculated by the numerical integration process given a fixed frequency, 2 MHz, exactly at the Rayleigh angle for three values of the beam width: 12 mm, 20 mm, and 28 mm. The results are plotted in Fig. 9 as three solid curves all having an intensity minimum between two intensity peaks. As indicated by these curves, when the beam width becomes larger, the complete profile gradually shifts to the left together with the intensity null while the right peak gains in intensity and the left one loses in intensity. The most noticeable change comes from the shift of the intensity null, which is displaced to the left by 17% of $2w_o$ as the latter is changed from 12 mm to 20 mm. For incidence at the Rayleigh angle, the same reflected beam profile can be calculated using the Bertoni and Tamir formulation with attenuation taken into account. These results are presented in the same figure in the form of broken curves. Agreement between two sets of curves is seen to be reasonable with the discrepancy estimated at the intensity peaks to be about 2.5% on the average. The outcome indicates that the Bertoni and Tamir formulation is an excellent approximation for the description of the non-specular reflection phenomena at the Rayleigh angle provided that the physical parameters entered are sufficiently accurate. The numerical integration method is more dependable in view of the advantage that the calculation error is almost non-existent.

2. Variation of Beam Profile with Sound Frequency

The sound frequency strongly affects the reflected beam profile constructed by (23) through the attenuation parameters in $R(A_x)$ and the normalized half beam width W in $V(A_x)$ and $E(A_x)$. The relationship between the reflection coefficient and attenuation has been discussed in

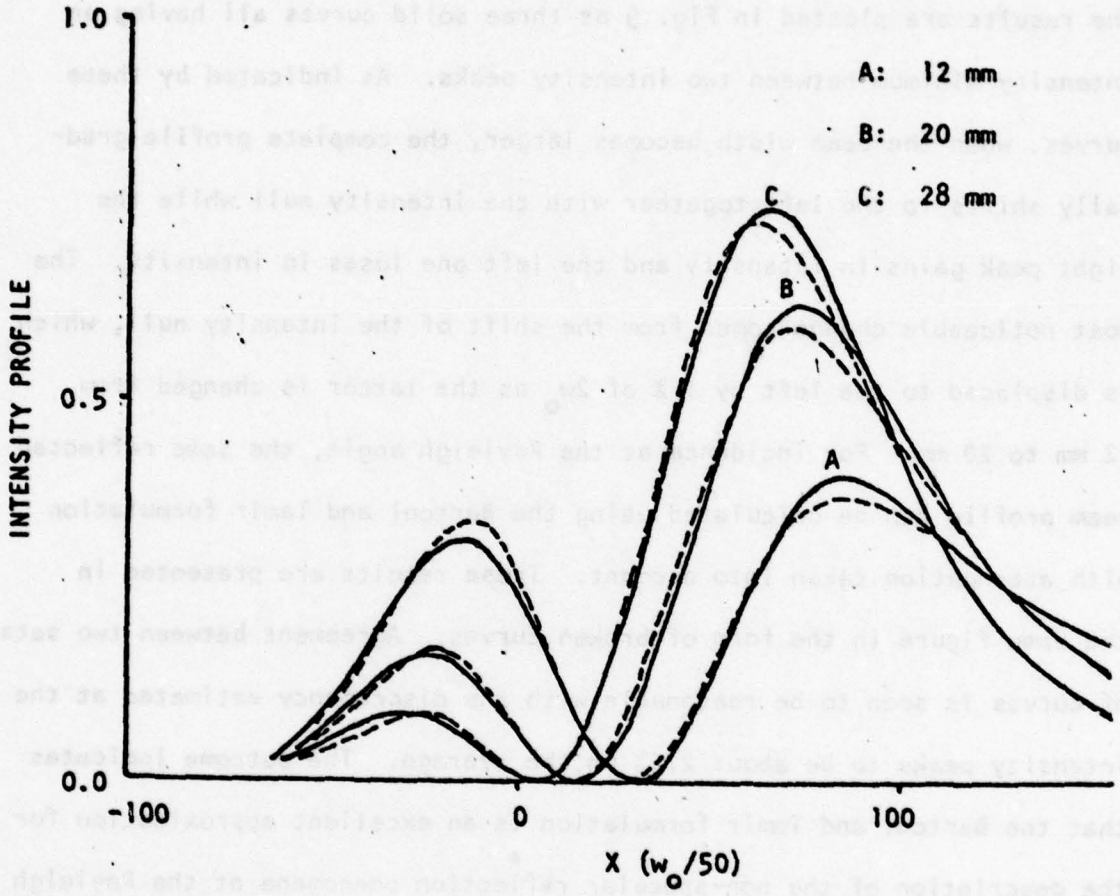

Figure 9. Reflected beam profiles for a water-stainless steel interface at Rayleigh angle incidence with the same frequency (2 MHz) but different beam width. The solid curves are calculated by the numerical integration method while the broken ones are produced by the Bertoni and Tamir formulation.

detail in Chapter II. The numerical integration method is now used to calculate the reflected profile for a fixed beam width but different sound frequencies. Figure 10 shows these profiles for a sound frequency of 1 MHz, 2 MHz, and 6 MHz and a beam width of 20 mm for incidence at the Rayleigh critical angle.

It is observed from the solid curves that the profiles are changed substantially as the sound frequency changes. Again the profiles exhibit two intensity peaks and an intensity null. As the frequency is changed from 1 MHz to 2 MHz, the whole profile shifts to the left, with the right peak becoming higher and the left one smaller, while the null strip moves to the left by 22% of $2w_o$. At 6 MHz, one sees the same changing tendencies except that the left peak becomes so small that it almost disappears. In the same figure, the reflected beam profiles produced from the Bertoni and Tamir formulation are also drawn. Again they are seen to agree with the results of the numerical integration method and the approximation error involved can be estimated to be about 3% at the intensity peaks.

3. Variation of Beam Profile with Angle of Incidence

The numerical integration formulation is now applied to investigate changes in the reflected beam profile as the angle of incidence is varied about the Rayleigh critical angle. This is the case where the formulation suggested by Bertoni and Tamir is not fully applicable. It does not provide accurate results for angles of incidence other than the Rayleigh angle; the farther from it, the more erroneous the Bertoni and Tamir results become.

Because the reflected profile exhibits different patterns for

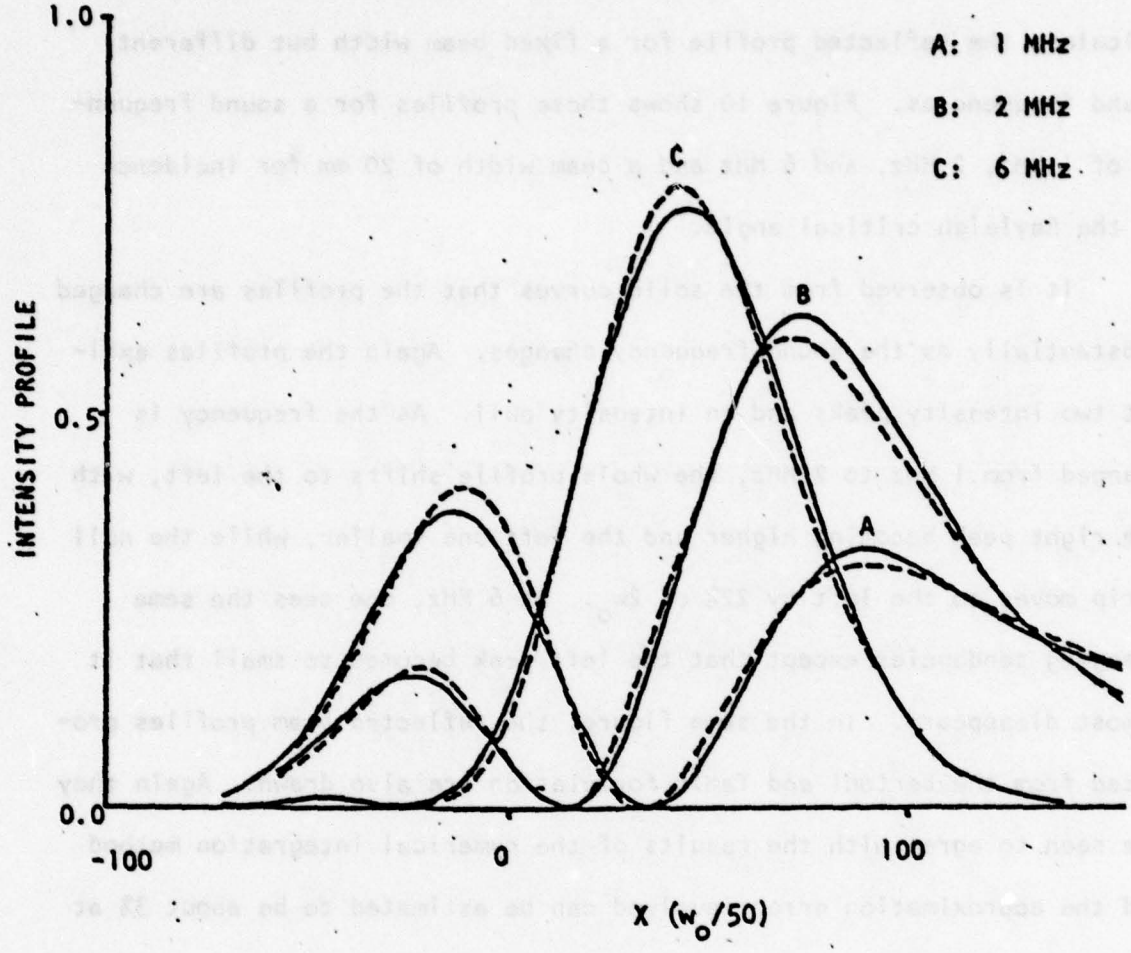

Figure 10. Reflected beam profiles for a water-stainless steel interface at Rayleigh angle incidence with the same beam width (20 mm) but different frequency. The solid curves are calculated by the numerical integration method while the broken ones are produced by the Bertoni and Tamir formulation.

different frequency ranges, calculations are done for two particular cases. In one case, the frequency and beam width are chosen to be 2 MHz and 20 mm; in the other, they are 15 MHz and 20 mm. In both situations, the angle of incidence is varied in steps of 0.25°.

Figure 11 illustrates the 2 MHz case with five reflected profiles indicating gradual changes as the angle of incidence is slowly increased above the Rayleigh angle. It can be observed from the figure that the changing profile is characterized by the following developments: (i) The intensity minimum remains essentially at the same position but its intensity slowly increases until it is completely flattened out approximately at 1° above the Rayleigh angle; (ii) The right peak slowly loses its intensity and the left one becomes larger until they gradually merge into one; and (iii) Beyond 1° above the Rayleigh angle, the original reflected profile turns into a Gaussian one whose only remaining non-specular feature is a small beam displacement.

The results for 15 MHz are presented in Figs. 12 and 13. The reflected profile now is found to have a simpler nature. The non-specular reflectivity is manifest only in a lateral shift of the beam. Figure 12 shows the gradual changes in the reflected beam profile as the angle of incidence becomes less than the Rayleigh angle: (i) The beam displacement becomes smaller; and (ii) The maximum peak becomes more intense as the extent of non-specular reflectivity is no longer noticeable at more than 2° away from the critical angle. The beam displacement and peak intensity are plotted in Fig. 13 as functions of the angle of incidence.

In both situations, additional calculations were done for angles of incidence smaller than the Rayleigh angle in the 2 MHz case and larger

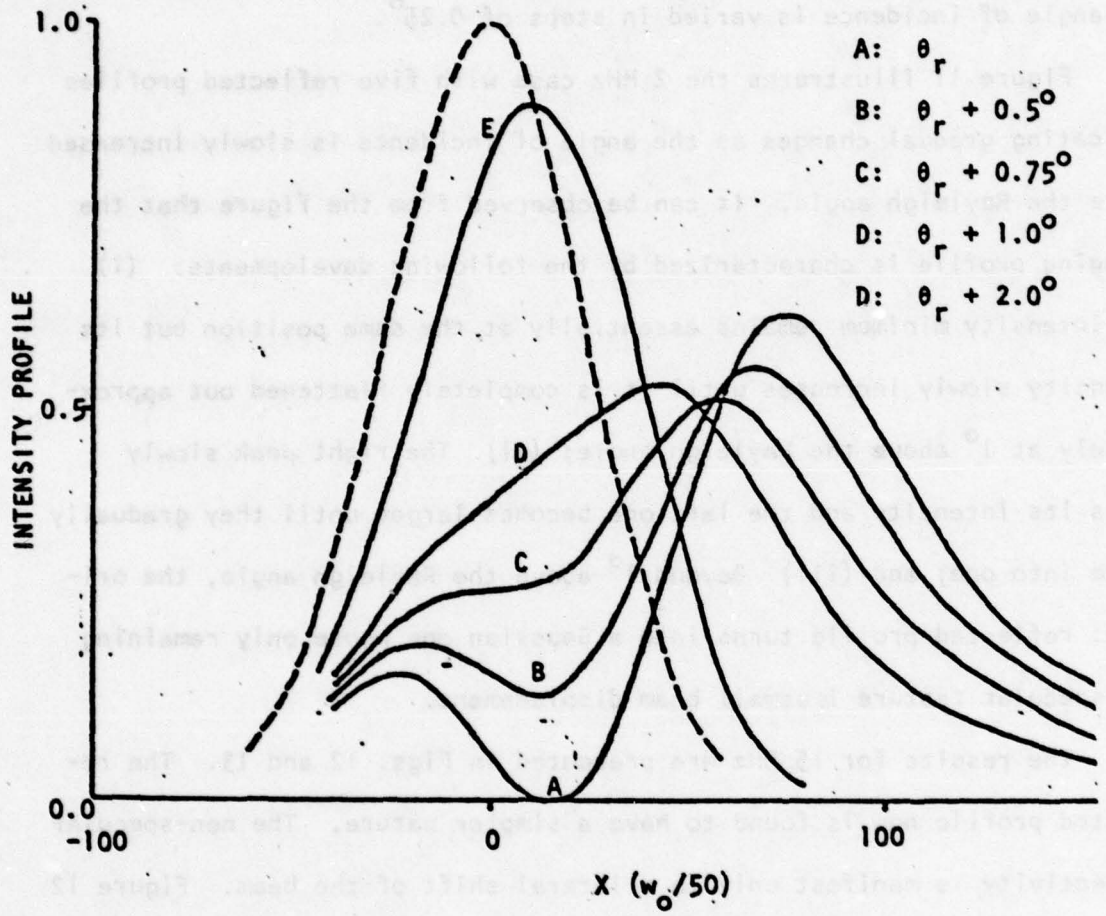

Figure 11. Reflected beam profiles calculated by the numerical integration method for a water-stainless steel interface when the incident angle is varied slightly from the Rayleigh angle and the frequency and beam width remain the same (2 MHz and 20 mm). The broken curve is the incident beam profile.

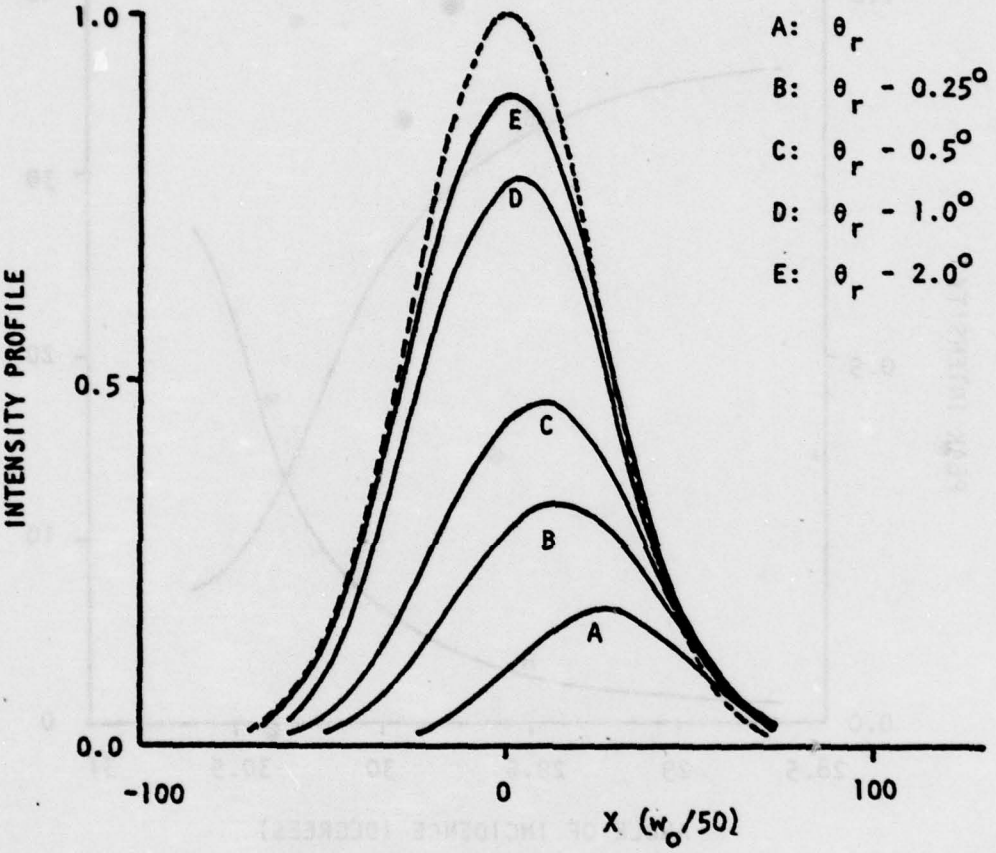

Figure 12. Reflected beam profiles calculated by the numerical integration method for a water-stainless steel interface when the incident angle is varied slightly from the Rayleigh angle and the frequency and beam width remain the same (15 MHz and 20 mm). The broken curve is the incident beam profile.

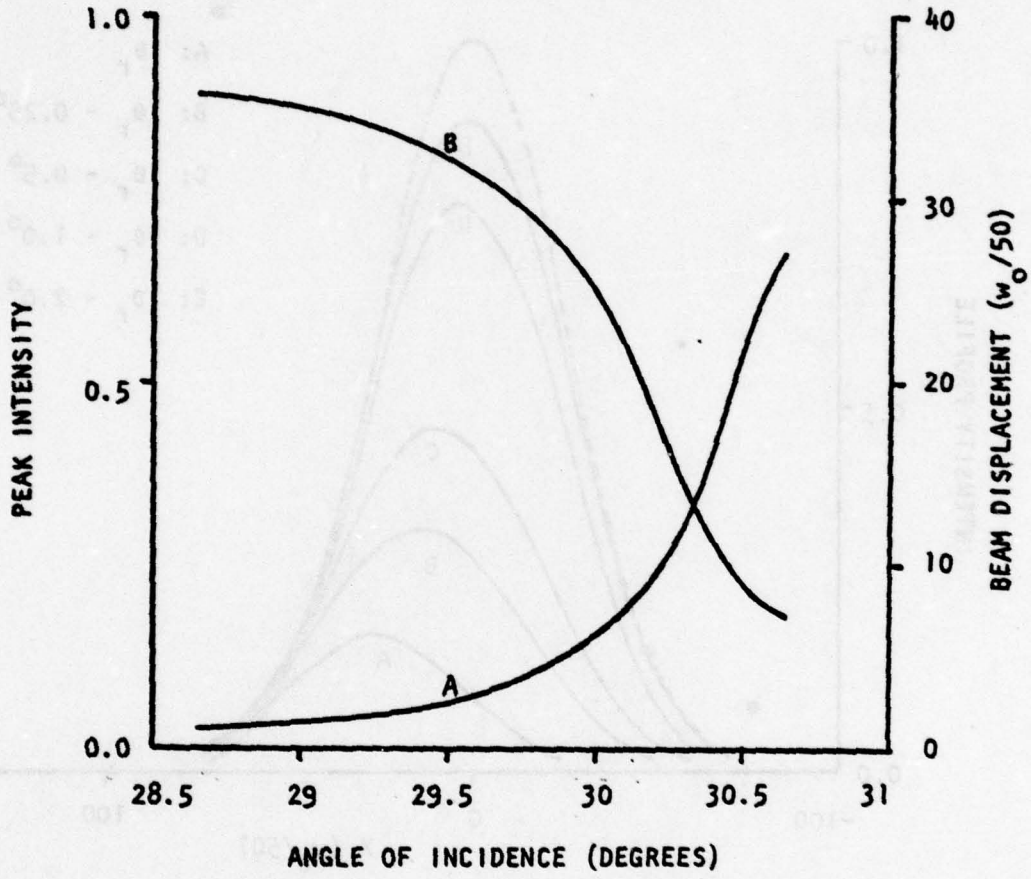

Figure 13. Beam displacement (A) and peak intensity (B) of the reflected beam profiles near the Rayleigh angle for a water-stainless steel interface as functions of the incident angle. The sound frequency and beam width are 15 MHz and 20 mm, respectively.

in the 15 MHz case. The results are found to be almost identical to the profile changes described above. It can be concluded that non-specular reflection effects near the Rayleigh angle are most pronounced at the Rayleigh angle and become less so as the angle of incidence departs from the critical angle. However, the effects are still observable as far as 2^{o} away from the Rayleigh angle.

B. Reflected Profile for Incidence near Longitudinal Critical Angle

The results arising out of the investigation of the absorptive plane wave reflection coefficient also lead to the belief that non-specular reflectivity may exist near the longitudinal critical angle. The reflected beam profile for that critical angular range can also be determined by the numerical integration method. Again the reflected profile is calculated for different parameters, including the sound frequency, the beam width, and the angle of incidence.

In this section, all calculations are done for a water-Plexiglas interface. The choice of this liquid-solid combination is made in accordance with earlier observations, discussed in Chapter II, about the plane wave reflection coefficient: in the case of a water-Plexiglas interface, $R(k_x)$ exhibits strong variations in magnitude and phase near the longitudinal critical angle. As a result, preliminary calculations show that at the longitudinal critical angle, the reflected beam profile for a water-stainless steel interface is only slightly displaced by about 2% of $2w_o$, in contrast to the case of water-Plexiglas, where the displacement becomes much greater and can be readily observed experimentally.

1. Variation of Beam Profile with Beam Width

The reflected profile is calculated by the numerical integration

formulation at the longitudinal critical angle for a fixed frequency, 2 MHz, with different values of the beam width: 12.7 mm, 19.1 mm, and 25.4 mm. The non-specular reflectivity is shown by a distinct beam displacement, which is calculated to be 14%, 13%, and 11% of $2w_o$ for 12.7 mm, 19.1 mm, and 25.4 mm, respectively. The complete profiles for these values are plotted in Fig. 14. It is seen that, as the beam width becomes larger, the beam displacement decreases and the peak intensity increases.

2. Variation of Beam Profile with Sound Frequency

The reflected beam profile is calculated for different values of the sound frequency. The beam width is constant (19.1 mm) and the angle of incidence is the longitudinal critical angle. Figure 15 shows the reflected beam profiles for three cases: 1 MHz, 2 MHz and 6 MHz. Again, the only non-specular feature seen in the figure is a lateral shift of the reflected beam: 11%, 13%, and 4% of $2w_o$ for 1 MHz, 2 MHz, and 6 MHz, respectively. Because of lack of attenuation data for other frequencies, only these three mentioned profiles are calculated and thus sufficient evidence is not available to reach a conclusion regarding variation of the beam displacement and the peak intensity as functions of the sound frequency. However, it can be assumed that there might exist a certain frequency between 2 MHz and 6 MHz where the beam displacement and intensity peak would reach a maximum.

3. Variation of Beam Profile with Angle of Incidence

Figure 3 in Chapter II shows that near the longitudinal critical angle the reflection amplitude is strongly dependent on the angle of incidence, increasing from 40% to 100% reflection within less than 2^o

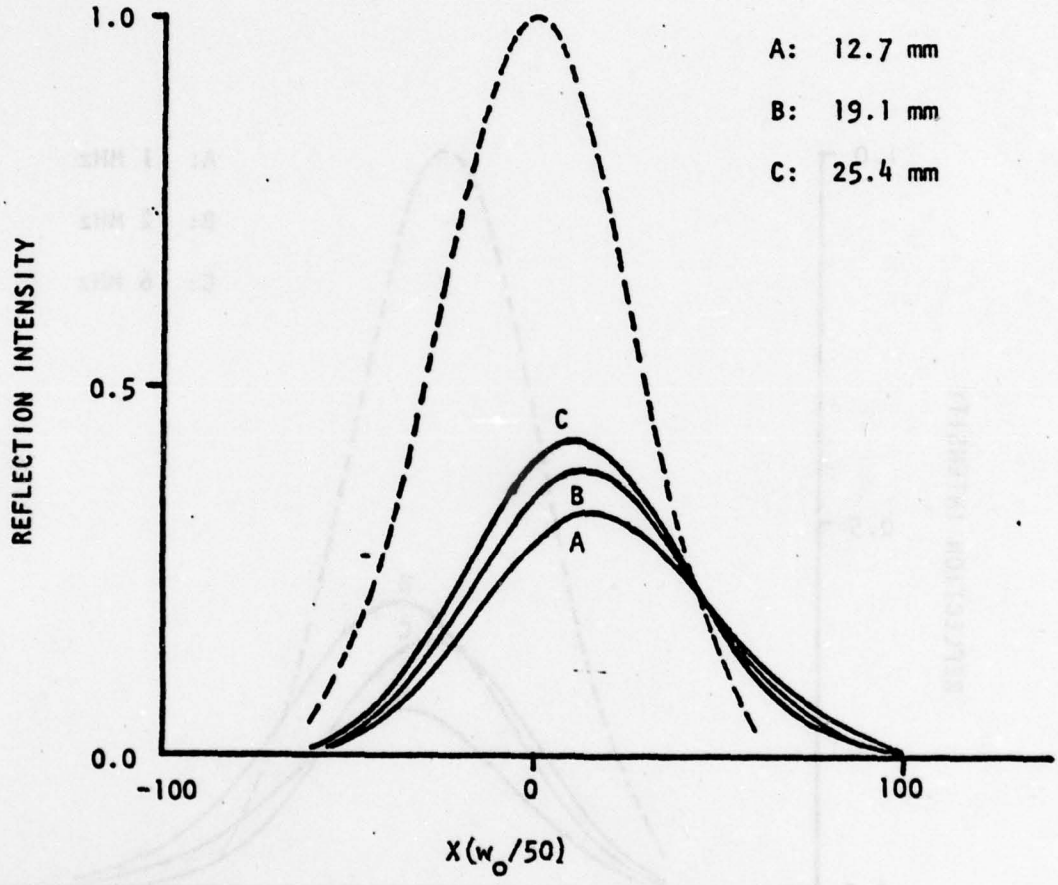

Figure 14. Reflected beam profiles calculated by the numerical integration method at the longitudinal critical angle for a water-Plexiglas interface with the same frequency (2 MHz) but different beam width. The broken curve is the incident beam profile.

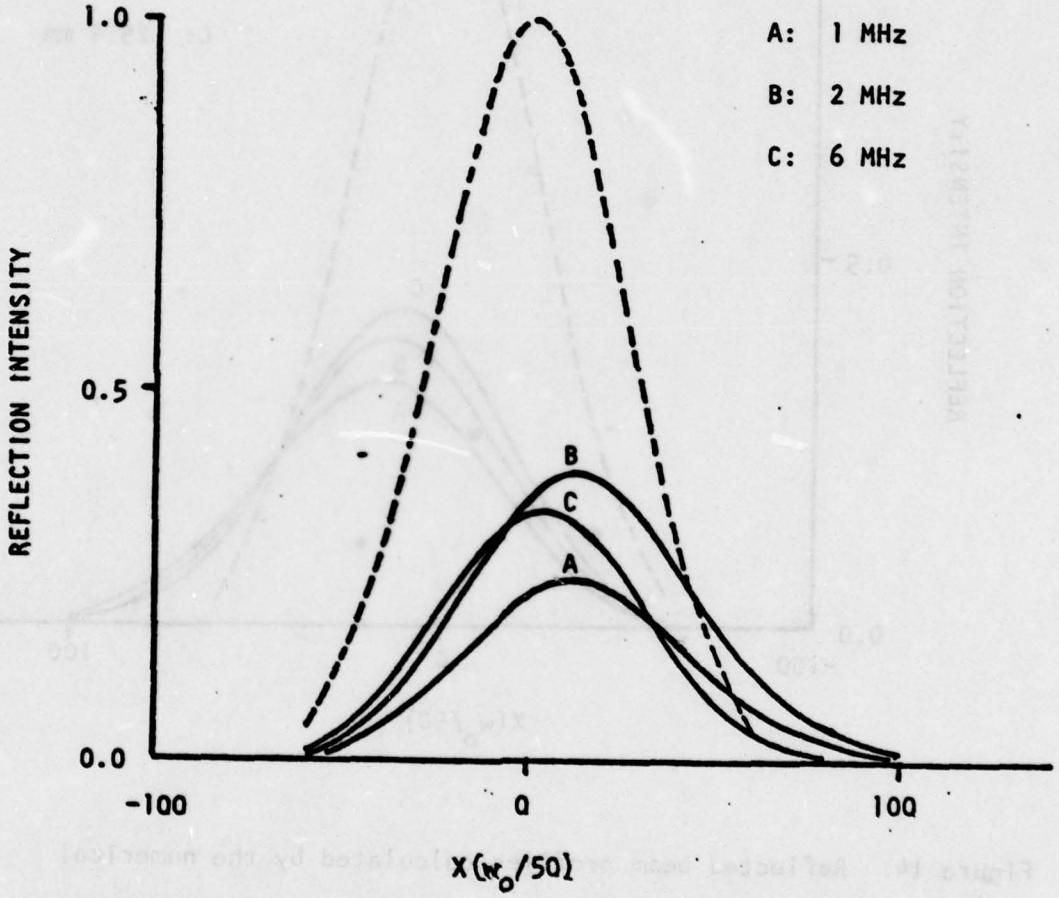

Figure 15. Reflected beam profiles calculated by the numerical integration method at the longitudinal critical angle for a water-Plexiglas interface with the same beam width (19.1 mm) but different frequency. The broken curve is the incident beam profile.

change. Expectedly, the reflected profile would vary appreciably in this angular range. The numerical integration method is now used to determine the reflected profile of a beam of 2 MHz frequency and 19. 1 mm width when the angle of incidence is varied by steps of 0.5° about the longitudinal critical angle. Some of these profiles are shown in Fig. 16 for incident angles between θ_d and $\theta_d + 3^{\circ}$. It can be seen that the variation of the beam displacement and peak intensity are substantial only near the longitudinal critical angle.

To obtain a more detailed knowledge of the relationship between the beam displacement and the angle of incidence, calculations are done for smaller increments of the incident angle. The calculated results shown by the solid curves in Fig. 19 in Chapter V indicate that there exists a sharp increase in both the beam displacement and the peak intensity approximately at $\theta_d - 0.5^{\circ}$. They both reach a maximum not at θ_d but at about 1° above it. These theoretical predictions are consistent with experimental measurements described in Chapter V.

It is instructive to compare the above profile changes to those described in Fig. 12 for the water-stainless steel interface at 15 MHz near the Rayleigh critical angle. In both cases, one notes that the beam displacement increases as the critical angle is approached. However, the peak intensity rises in the water-Plexiglas case and decreases in the water-stainless steel case. In view of these observations and the known behavior of $R(k_x)$, one may arrive at the following association: the peak intensity largely expresses the variation of the reflection amplitude while the beam displacement changes proportionally with the gradient of the phase shift generated upon reflection.

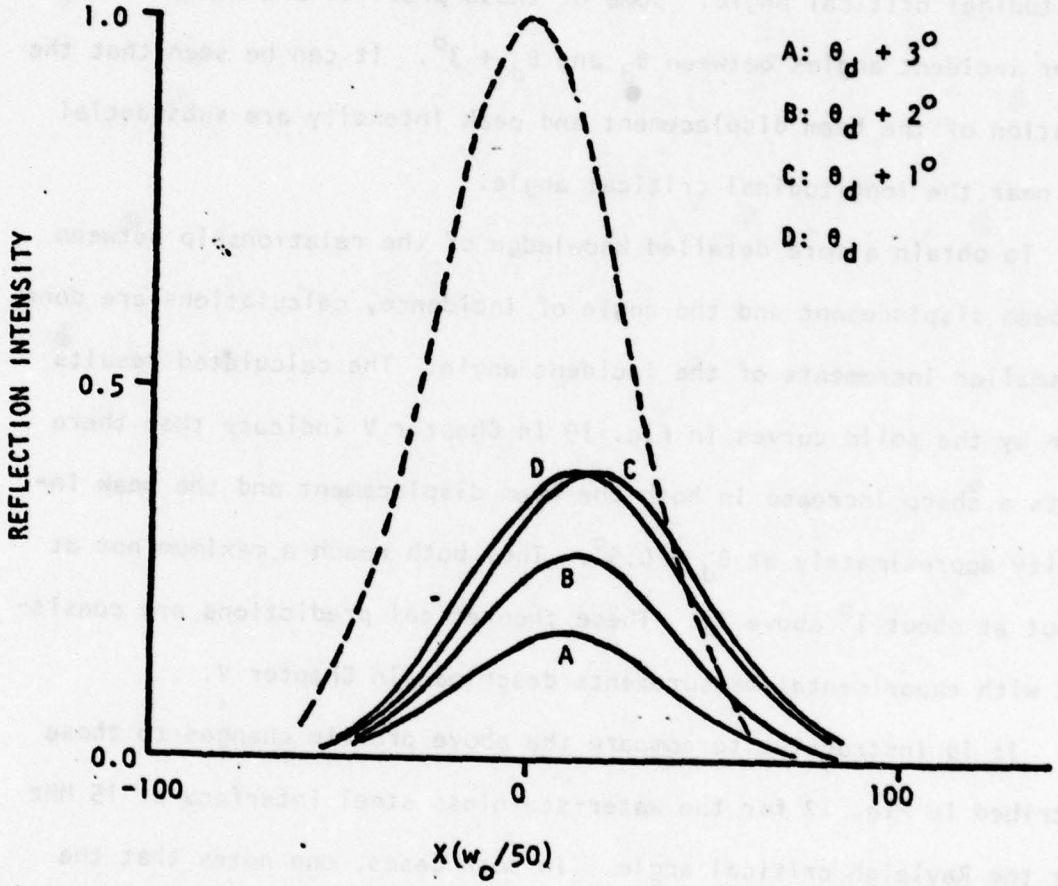

Figure 16. Reflected beam profiles calculated by the numerical integration method for a water-Plexiglas interface when the incident angle is varied near the longitudinal critical angle. The sound frequency and beam width are 2 MHz and 19.1 mm, respectively.

CHAPTER V

EXPERIMENTAL INVESTIGATION OF NON-SPECULAR REFLECTIVITY

In the previous chapters, the theoretical aspects of the problem of non-specular reflectivity have been studied in detail, first by examining the plane wave reflection coefficient, and then by discussing various formulations for determining the reflected beam profile. Experimental evidence of the non-specular reflection phenomena has been reported by several authors [3,7], mostly for incidence at the Rayleigh critical angle. With the numerical integration method and by taking proper account of attenuation in the media, the non-specularly reflected profile can now be described rather accurately for all angles of incidence.

A. Scope of Investigation

The principal objectives of the present experimental investigation can be summarized as follows:

(i) Study the profile changes of the reflected beam when the angle of incidence is slowly varied around the Rayleigh critical angle for a water-stainless steel interface.

(ii) Monitor the changes in the reflected beam profile for incidence near the longitudinal critical angle onto a water-Plexiglas interface. A detailed investigation of the beam displacement and peak intensity is undertaken in this case to verify earlier theoretical results.

B. Experimental Procedures

The development of the experimental procedures used here is centered around two standard techniques: the Schlieren imaging technique to visualize the path of a bounded sound beam, and the pulse-echo method to measure attenuation in materials. The experimental work proceeds in the following steps:

(i) Determination of the attenuation parameters

For a specific sample, its geometrical dimensions are measured and, together with its mass, are used to determine its density and the length of the travel path of the sound pulse through the sample. Next, the conventional attenuation constant, α, and the sound velocity are determined by the pulse-echo technique for a given sound frequency. These results are used to calculate attenuation parameters according to (4). The same measurements are done for both longitudinal and shear waves.

(ii) Study of the profile changes for a water-stainless steel interface near the Rayleigh critical angle

A Schlieren imaging experiment is set up to observe the incident and reflected sound beam for a stainless steel sample immersed in water. The steel sample is 25.4 mm thick and thus can be considered to be a half-space. For the frequencies used, the sample surface is polished to eliminate effects of a rough surface. After the sound frequency and the beam width are chosen, the angle of incidence is slowly varied about the Rayleigh critical angle. The continuously changing beam profile is first recorded by a video cassette player providing a preliminary survey of the significant features of non-specular reflection phenomena. The angular scanning of the reflection repeated and this time

still photographs are taken of the complete beam profile at 0.5° increments of the incident angle, including the critical angle.

(iii) Study of the profile changes for a water-Plexiglas interface near the longitudinal angle

The same procedure as described in step (ii) is employed. The sample thickness again is 25.4 mm and thus would qualify as a half-space. The only difference is that the angle of incidence now is varied in the neighborhood of the longitudinal critical angle. The still photographs of the beam profile are also taken by 0.5° steps. In addition, a more detailed verification of the theoretical results predicted by the numerical integration method is attempted through a closer measurement of the beam displacement. This is achieved by taking more photographs of the beam profile with finer increments of the angle of incidence and measuring the beam displacement. The displacement is the distance between the point where the intensity peak of the incident beam strikes the interface and the point of reflection of the intensity peak of the reflected beam.

C. Results and Analyses

1. Attenuation Data

Attenuation data for Plexiglas are obtained in the manner described in step (i) above. The sound frequencies used for both longitudinal and shear measurements are 1 MHz, 2 MHz, and 5 MHz. Interpolation of the measured values of the longitudinal and shear attenuation constants provides the complete set of data given in Table 2. The measured sound velocities in Plexiglas are listed in Table 1. The interpolation process is achieved by fitting the experimentally obtained values to the

curve represented by

$$\ln \alpha = a \ln f - b , \tag{24}$$

where f is measured in MHz and α in neper per meter. For the shear attenuation, the coefficients are estimated to be a = 3.218 and b = 2.631, and for the longitudinal attenuation a = 2.280 and b = 2.659.

Attenuation data for stainless steel are derived from measurements by Fitch [10] for the longitudinal and shear attenuation constants. These values are again fitted by the same method and are extrapolated to 40 MHz. The coefficients in this case are found to be a = 1.614, b = 2.661 for the shear attenuation and a = 1.334, b = 2.626 for the longitudinal attenuation. For water, the attenuation constant is taken to be a linear function of the sound frequency at room temperature in the frequency range of interest. As a result, the attenuation parameter of water is frequency-independent, as shown in Table 2.

2. Profile Changes for Water-Stainless Steel Interface

The reflected beam profile is observed for the water-stainless steel interface near the Rayleigh angle, following the procedure of step (ii). The beam width and the sound frequency used are 20 mm and 2 MHz, respectively. Figure 17 shows five Schlieren photographs of the sound beam being reflected at the interface. They indicate a reasonable agreement with the theoretically calculated profiles described in Fig. 11. As the angle of incidence is increased from 1° below the Rayleigh angle to 1° above it, the dark strip representing the intensity null is first dimly visible, becomes clearest approximately at the Rayleigh angle, and slowly disappears again beyond the Rayleigh angle.

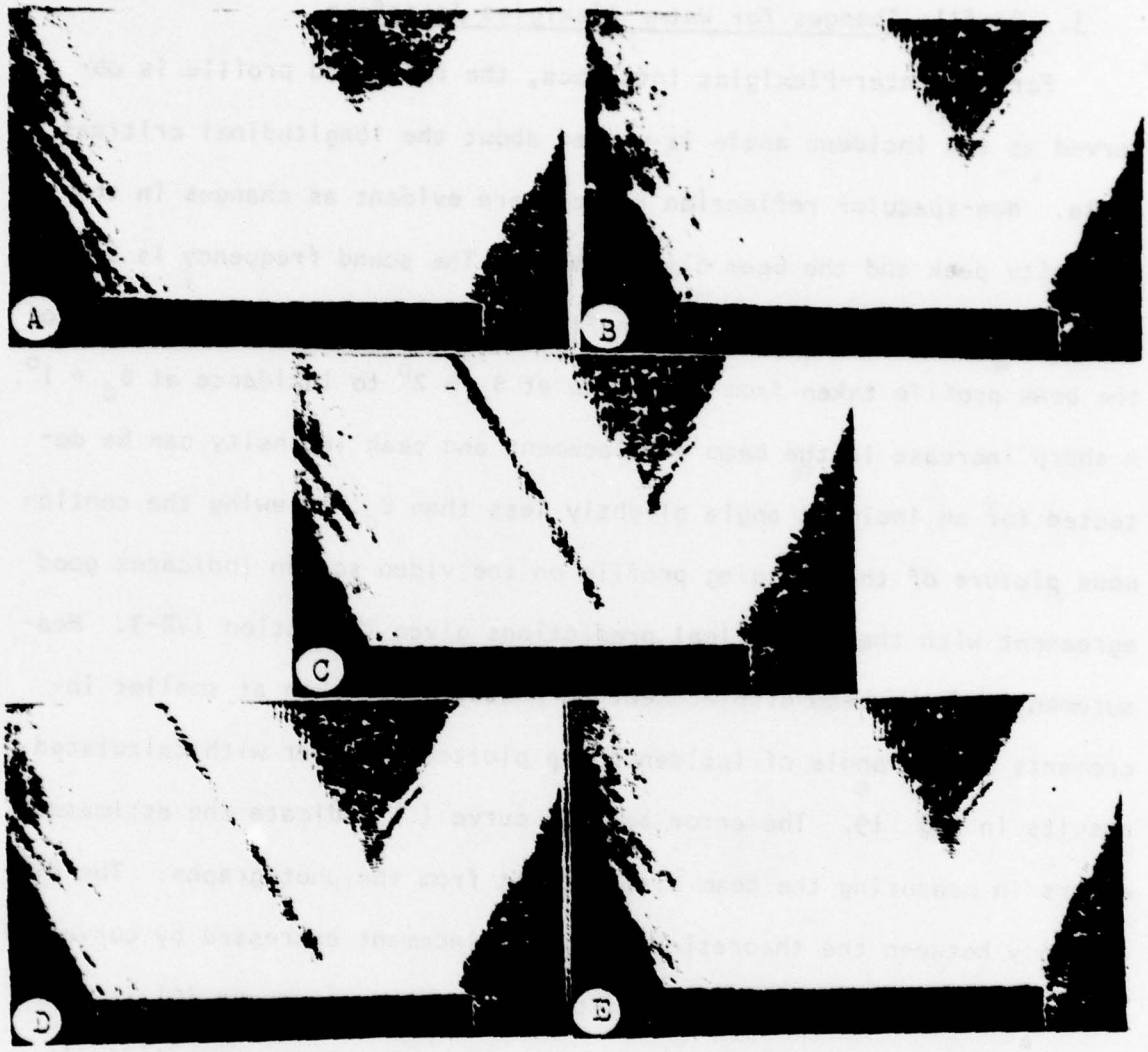

Figure 17. Schlieren photographs showing gradual change in the reflected beam profile for a water-stainless steel interface with the angle of incidence being (A) $\theta_r - 1^o$, (B) $\theta_r - .5^o$, (C) θ_r, (D) $\theta_r + .5^o$, and (E) $\theta_r + 1^o$.

3. Profile Changes for Water-Plexiglas Interface

For the water-Plexiglas interface, the reflected profile is observed as the incident angle is varied about the longitudinal critical angle. Non-specular reflection effects are evident as changes in the intensity peak and the beam displacement. The sound frequency is 2 MHz and the beam width is 19.1 mm. In Fig. 18 are shown four photographs of the beam profile taken from incidence at $\theta_d - 2^\circ$ to incidence at $\theta_d + 1^\circ$. A sharp increase in the beam displacement and peak intensity can be detected for an incident angle slightly less than θ_d. Viewing the continuous picture of the changing profile on the video screen indicates good agreement with the theoretical predictions given in section IVB-3. Measurements of the beam displacement on photographs taken at smaller increments of the angle of incidence are plotted together with calculated results in Fig. 19. The error bars on curve (C) indicate the estimated errors in measuring the beam displacement from the photographs. The discrepancy between the theoretical beam displacement expressed by curve (B) and the experimentally measured displacement shown by curve (C) is due to the fact that the shear wave velocity and attenuation are difficult to measure to a high degree of accuracy. However, it is significant to note that both calculated and experimental curves exhibit the same variation pattern for the beam displacement as a function of the angle of incidence.

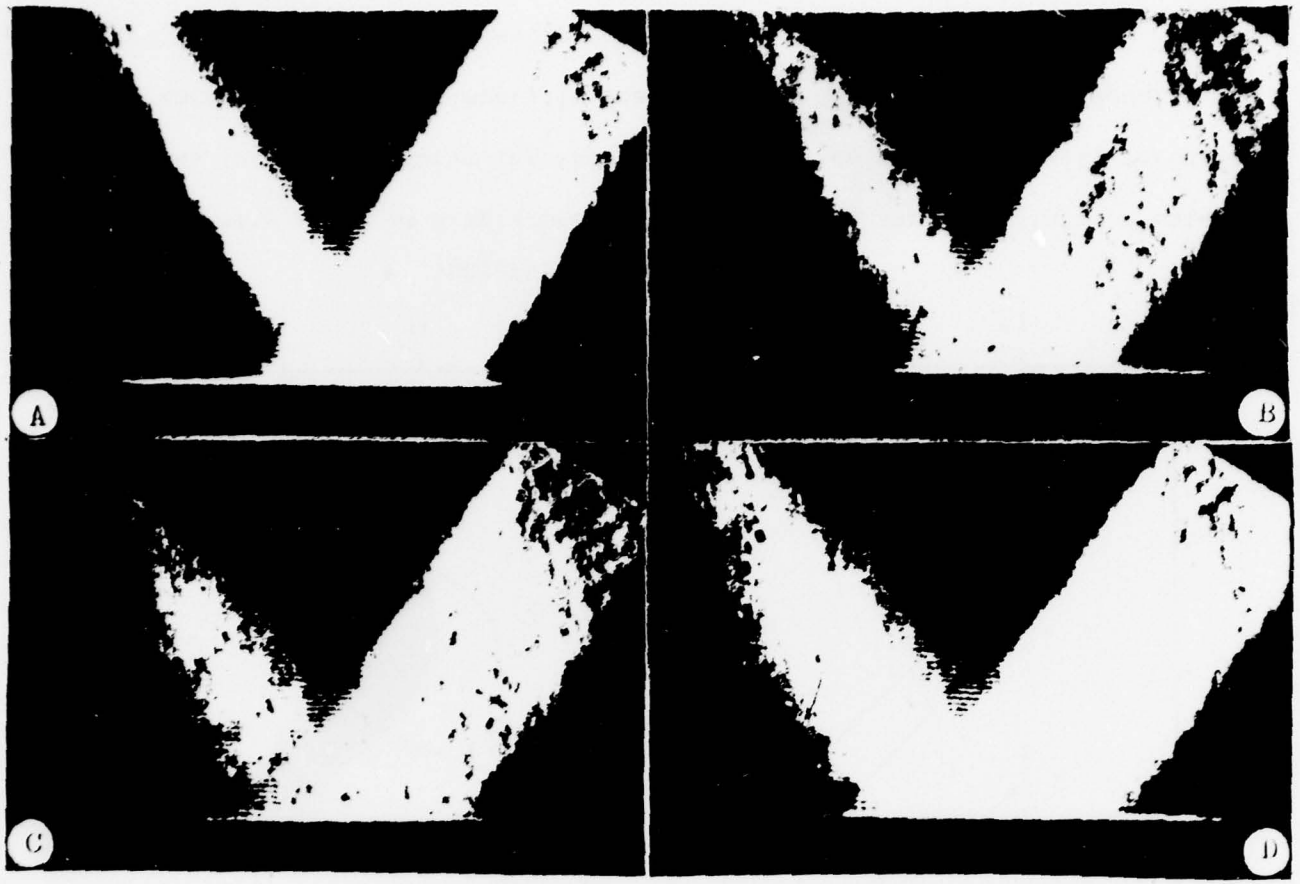

Figure 18. Schlieren photographs showing change in the reflected beam profile in the form of a beam *displacement* near the longitudinal critical angle. The angle of incidence is (A) $\theta_d - 2^o$ (B) $\theta_d - 1^o$, (C) θ_d, and (D) $\theta_d + 1^o$.

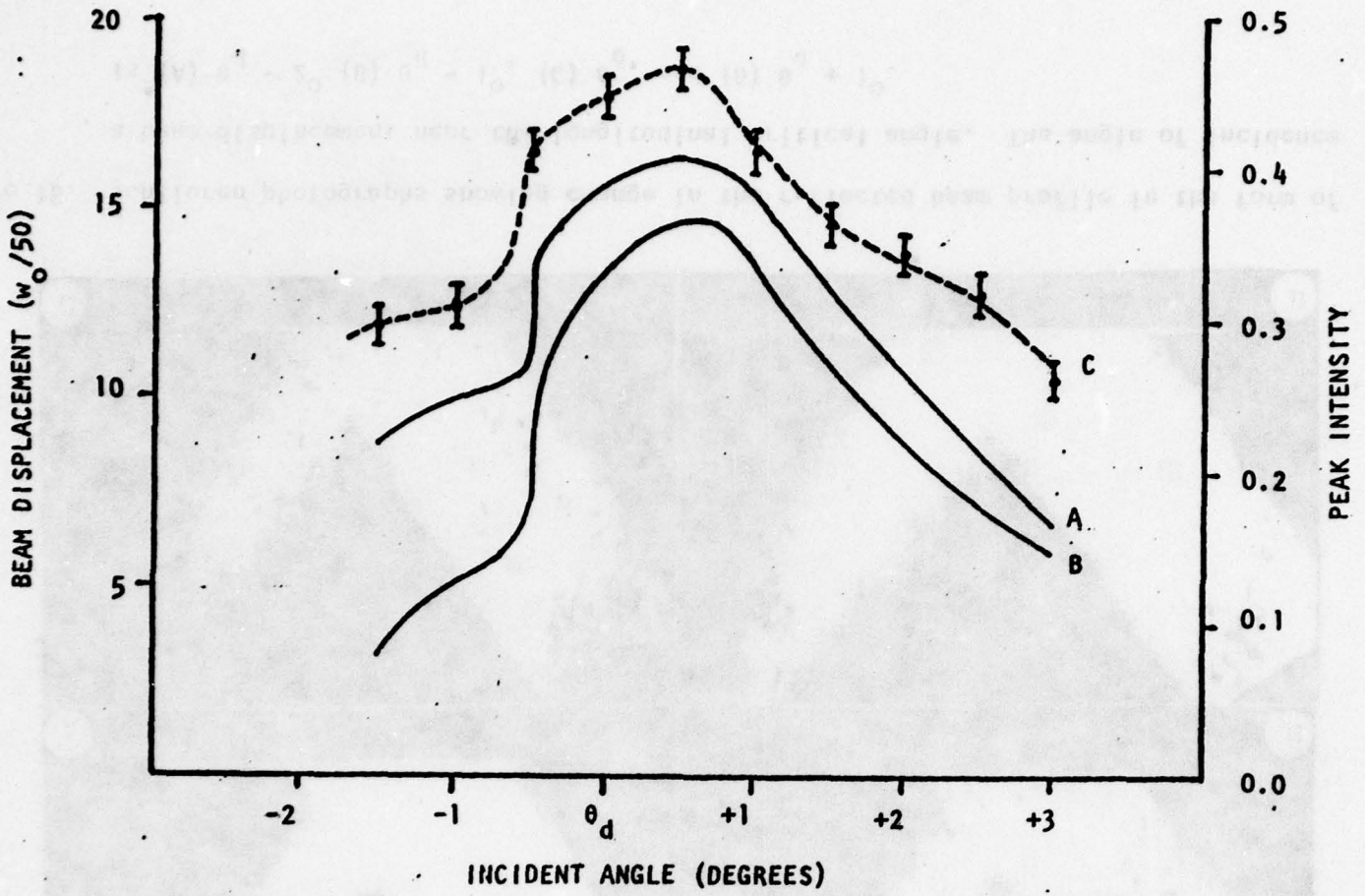

Figure 19. Peak intensity and beam displacement between $\theta_d - 2^o$ and $\theta_d + 3^o$ for a water-Plexiglas interface. Curve (A) shows the theoretical peak intensity variation. The theoretical and experimentally measured beam displacements are denoted by curves (B) and (C), respectively.

CHAPTER VI

CONCLUSIONS

The previous chapters have been devoted to a theoretical analysis and an experimental investigation of the profile of a bounded ultrasonic beam reflected from a liquid-solid interface. A numerical integration method has been employed to calculate the reflected beam profile for the complete range of incident angles. Detailed results were obtained by this method with different parametric conditions for two particular cases: incidence near the Rayleigh angle onto a water-stainless steel interface and incidence near the longitudinal critical angle onto a water-Plexiglas interface. It was found that calculated profiles agreed reasonably well with experimental results provided by the Schlieren visualization technique.

The investigation has led to the following major results, possible further investigations and remaining unsolved questions:

(i) With a rigorous account of attenuation in the media, the numerical integration method presents an accurate theoretical model to determine the profile of a bounded ultrasonic beam reflected from a liquid-solid interface as a function of the sound frequency, the beam width, and the angle of incidence. The most significant contribution of this method is that it allows computation of the profile for any angle of incidence instead of being restricted to non-specular reflection phenomena at the Rayleigh angle. This aspect is demonstrated by the result

obtained in the present work for the case of a water-Plexiglas interface in which non-specular reflectivity is shown to exist near the longitudinal critical angle and can be described in quantitatively satisfactory detail.

(ii) Methodologically, the numerical integration method affirms that spectral representation is a sound mechanism to express the boundedness of an ultrasonic beam. It entails a physical interpretation of the beam profile as the interference of an infinite number of infinite plane waves, of which non-specular reflectivity at the Rayleigh angle is a particular case that enables one to view the reflected profile as a product arising out of a "resonance" situation.

(iii) In view of the practical potential of the numerical integration method, the present research can be extended in several directions. First, the numerical approach could be applied to study the non-specular reflectivity problem for other structures of layered media, such as a solid plate immersed in a liquid, of which the reflected beam profile has been established for plate-mode incidence. Second, on an equivalent footing, the non-specular transmittivity phenomena could be investigated in a systematic way by the same method again for different layered structures. Third, thanks to its numerical formulation, the numerical integration method could be modified with relative ease to accommodate non-Gaussian profiles, which may be encountered more often in practice. And finally, the same approach could be extended to study the so-called beam spreading and diffraction effects: "beam spreading" describes a phenomenon in which a bounded beam is frequently not well-collimated but gradually diverges as it travels in a medium; and

"diffraction" indicates a diffraction-like beam profile when observed away from the active surface.

(iv) As was noted earlier, the spectral representation principle implies that a bounded incident beam is constructed from a superposition of infinite plane waves all having different wave vectors. With the y component being eliminated in the current formulations, the difference between the wave vectors of these individual plane waves is manifest in the form of either different sound frequencies or a perturbation in the angle of incidence. Reformulation of the numerical integration method to explicitly consider this difference may help understand the real physical structure of a bounded ultrasonic beam. This represents a new problem which is yet to be solved and may involve some aspects of nonlinear acoustics.

APPENDICES

FORTRAN IV COMPUTER PROGRAMS USED IN THEORETICAL CALCULATIONS

A. Magnitude and Phase of Reflection Coefficient

```
C      REFLECTION COEFFICIENT FOR ABSORPTIVE L/S STRUCTURE
C            20 C WATER/STAINLESS STEEL
C      INPUT PARAMETERS
       P=3.141592654
       V=1.48
       VD=5.84
       VS=3.13
C      CRITICAL ANGLES EVALUATED
       TAND=SQRT((V/VD)**2/(1-(V/VD)**2))
       TANS=SQRT((V/VS)**2/(1-(V/VS)**2))
       THETAD=ATAN(TAND)
       THETAS=ATAN(TANS)
       PS=.5*(VD**2-2*VS**2)/(VD**2-VS**2)
       VR=VS*(.87+1.12*PS)/(1+PS)
       TANR=SQRT((V/VR)**2/(1-(V/VR)**2))
       THETAR=ATAN(TANR)
       TD=THETAD*180/P
       TS=THETAS*180/P
       TR=THETAR*180/P
       WRITE (6,30)
       WRITE (6,35) TD,TS,TR
C      INPUT ATTENUATION PARAMETERS
  05   READ (5,40) F,C2,C3
       IF (C2.LT.0.0)  GO TO 06
       WRITE (6,45)
       WRITE (6,40) F,C2,C3
C      SUBROUTINE CALLED TO PRINT OUT AMPLITUDE & PHASE
       THETA=.45
       STEP=1
       CALL IMP(THETA,STEP,F,C2,C3)
       THETA=THETAD*180/P
       STEP=.01
       WRITE (6,20)
       CALL IMP(THETA,STEP,F,C2,C3)
       THETA=THETAS*180/P
       WRITE (6,25)
       CALL IMP(THETA,STEP,F,C2,C3)
       THETA=THETAR*180/P
       WRITE (6,26)
       CALL IMP(THETA,STEP,F,C2,C3)
       GO TO 05
  06   STOP
20     FORMAT(// 5X,'DETAILED COMPUTATION AT LONG CRIT ANGLE'
25     FORMAT(//5X,'DETAILED COMPUTATION AT SHEAR CRIT ANGLE'
26     FORMAT(//5X,'DETAILED COMPUTATION AT RAYLEIGH CRIT ANG
30     FORMAT(//5X,'THETAD',9X,'THETAS',9X,'THETAR'/)
35     FORMAT(3E15.4//)
```

```
   40  FORMAT (10X,3F10.6)
   45  FORMAT(/10X,'FREQUENCY',2X,'LONG ATT',3X,'SHEAR ATT')
       END
```

```
       SUBROUTINE IMP(THETA,STEP,F,C2,C3)
       COMPLEX A(3),B(3),BP,BM,T1,T2,T3,R,CI
       DIMENSION V(3),C(3)
C      INPUT PARAMETERS
       V(1)=1.48
       V(2)=5.84
       V(3)=3.13
       P=3.141592654
       DI=0.1260716
       CI=(0.0,1.0)
       C(1)=0.00026/(2*P)
       C(2)=C2/(2*P)
       C(3)=C3/(2*P)
       DO 01 J=1,3
       A(J)=(V(1)/V(J))*CMPLX(1.0,C(J))
   01  CONTINUE
        WRITE (6,15)
C      EVALUATION OF REFLECTION MAGN & PHASE
       DO 02 K=1,89
       ZI=THETA-0.45+STEP*K
       AX=SIN(ZI*P/180)
       DO 03 L=1,3
       BP=A(L)+AX
       BM=A(L)-AX
       PP=ATAN2(AIMAG(BP),REAL(BP))
       PM=ATAN2(AIMAG(BM),REAL(BM))
       IF (PP.LT.0.0)  PP=PP+2*P
       IF (PM.LT.0.0)  PM=PM+2*P
       B(L)=SQRT(CABS(BP)*CABS(BM))*CEXP(CI*(PP+PM)/2)
   03  CONTINUE
       T1=(A(3)**2-2*AX**2)**2
       T2=4*B(2)*B(3)*AX**2
       T3=DI*(A(3)**4)*B(2)/B(1)
       R=(T1+T2-T3)/(T1+T2+T3)
        RMAG=CABS(R)
       RPH=ATAN2(AIMAG(R),REAL(R))*180/P
       IF (RPH.LT.0.0)  RPH=RPH+360
       WRITE (6,10) ZI,RMAG,RPH
   02  CONTINUE
       RETURN
   10  FORMAT(3E15.4)
   15  FORMAT(6X,'INC ANGLE',6X,'MAGNITUDE',10X,'PHASE'//)
       END
```

B. Locations of Rayleigh Pole-Zero Pair

```
C     DETERMINATION OF RAYLEIGH POLE/ZERO FOR L/S STRUCTURE
C          20 C WATER/STAINLESS STEEL
C               FREQ RANGE 1-40 MHZ
C
      COMPLEX A(3),B(3),CI,BPLS,BMNS
      COMPLEX D1,D2,D3,DD1,DD2,DD3,D,DD,AP,APP
      DIMENSION V(3),C(3)
C     SOUND VELS AND OTHER CONSTANTS
      DATA V(1),V(2),V(3)/1.48,5.84,3.13/
      CI=(0.0,1.0)
      P=3.141592654
      DI=0.1260716
      C(1)=0.00026/(2*P)
      WRITE (6,40)
C     INPUT ATTENUATION PARAMETERS
   01 READ (5,35) F,C2,C3
      C(2)=C2/(2*P)
      C(3)=C3/(2*P)
      IF (C(2).LT.0.0)  GO TO 31
C     DO LOOPS SCANNING INITIAL POINTS START HERE
      DO 20 I=1,6
      DO 15 J=1,6
      UP=0.5095+I*0.0005
      WP=-0.01+J*0.005
      AP=CMPLX(UP,WP)
      IC=1
C     NORMALIZED K'S AND KAPPAS
   05 CONTINUE
      DO 10 K=1,3
      A(K)=(V(1)/V(K))*CMPLX(1.0,C(K))
      BPLS=A(K)+AP
      BMNS=A(K)-AP
      PPLS=ATAN2(AIMAG(BPLS),REAL(BPLS))
      PMNS=ATAN2(AIMAG(BMNS),REAL(BMNS))
      IF (PPLS.LT.0.0)  PPLS=PPLS+2*P
      IF (PMNS.LT.0.0)  PMNS=PMNS+2*P
      B(K)=SQRT(CABS(BPLS)*CABS(BMNS))*CEXP(CI*(PPLS+PMNS)/2)
   10 CONTINUE
C     NUMERATOR AND ITS DERIVATIVE
C     POLE SEARCH
      D1=(A(3)**2-2*AP**2)**2
      D2=4*B(2)*B(3)*AP**2
      D3=DI*B(2)*(A(3)**4)/B(1)
      D=D1+D2+D3
```

```
      DABS=CABS(D)
      DD1=8*AP*(2*AP**2-A(3)**2)
      DD2=8*AP*B(2)*B(3)-4*(AP**3)*(B(3)/B(2)+B(2)/B(3))
      DD3=(D)*AP*(A(3)**4)/(A(1)**2-AP**2))*(B(2)/B(1)-B(1)/B(2))
      DD=DD1+DD2+DD3
C     NEWTON-RAPHSON STEPS
      APP=AP-D/DD
      DIFFR=REAL(APP-AP)
      DIFFI=AIMAG(APP-AP)
      IF ((ABS(DIFFR)+ABS(DIFFI)).LE.1.E-07) GO TO 25
      AP=APP
      IC=IC+1
      IF (IC.GT.15)  GO TO 15
      GO TO 05
15    CONTINUE
20    CONTINUE
      GO TO 30
25    WRITE (6,50) F,C2,C3,APP
      GO TO 01
30    WRITE (6,55)
      GO TO 01
31    STOP
35    FORMAT (10X,3F10.6)
40    FORMAT (/4X,'FREQ',6X,'LONG ATT',3X,'SHEAR ATT',4X,'REALPA
     17X,'IMAGPART'/)
50    FORMAT(3E12.4,2E15.7)
55    FORMAT (/5X,'CANT FIND POLE'/)
      END
```

C. Reflected Profile Calculated from Bertoni and Tamir Results

```
C     REFLECTED BEAM PROFILE FOR ABSORPTIVE L/S SYSTEM
C     BEAM WIDTH RANGES FROM 6 MM TO 14 MM
C     AT 2 AND 6 MHZ
      COMPLEX AP,AZ,R1,R2
C     WATER VEL=KM/SEC,BEAM WIDTH=MM,FREQ=MHZ
      V=1.48
      P=3.141592654
C     READ IN FREQ,POLE AND ZERO
   01 READ(5,20) F,APR,API,AZR,AZI
      IF (F.LT.0.0) GO TO 08
      WRITE (6,25)
      WRITE (6,20) F,APR,API,AZR,AZI
      DO 06 J=1,5
      W=6.0+2.0*(J-1)
      WRITE (6,30) W
      WRITE (6,10)
      AP=CMPLX(APR,API)
      AZ=CMPLX(AZR,AZI)
      W1=W/SQRT(1.0-APR**2)
      ALFAW=P*F*API*W1/V
C     NORMALIZED VINC AND VREFL
      DO 05 I=1,300
      X=-2*W1+I*W1/50
      GAMMA=ALFAW-X/W1
      R1=(APR-AZ)/(APR-AP)
      R2=(AP-AZ)/(AP-APR)
      R=1-SQRT(P)*ALFAW*EXP(GAMMA**2)*ERFC(GAMMA)
      VABS=CABS(R1+R2*R)
      VI=EXP(-2*(X/W1)**2)
      VR=VI*VABS**2
      WRITE (6,15) I,VI,VR
   05 CONTINUE
   06 CONTINUE
      GO TO 01
   08 STOP
   10 FORMAT (/2X,'X(W0/50)',5X,'VINC',11X,'VREFL'/)
   15 FORMAT (I10,2E15.6)
   20 FORMAT (10X,5F10.7)
   25 FORMAT (/15X,'FREQ',6X,'APR',7X,'API',7X,'AZR',7X,'AZI
   30 FORMAT (/10X,'W=',F5.1/)
      END
```

D. Reflected Profile Determined by Numerical Integration Method

```
C     REFLECTED BEAM PROFILE FOR ABSORPTIVE L/S SYSTEM
C     BY DIRECT INTEGRATION USING SIMPSON'S RULE
C     NEAR THE LONG CRITICAL ANGLE
C     FOR WATER/PLEXIGLASS INTERFACE
C
      COMPLEX CI,FNE,FNR,SUM2,SUM4,VR,VR1,VR2,VR3
C     DEFINE TWO FUNCTIONS IN THE INTEGRAND
      FNV(AX)=EXP(-(CF*(AX-AI)/2)**2)
      FNE(AX)=CEXP(CI*CF*AX*XN)
C     INPUT PARAMETERS
      N=60
      F=2.0E06
      V=1.48E03
      P=3.141592654
      CI=(0.0,1.0)
      THETA=32.69
      AI=SIN(THETA*P/180.0)
      DO 18 M=1,3
      W=2.54*0.25*(M+1)/2.0
      W=W*0.01
C     COMMON FACTORS
      WX=W/SQRT(1.0-AI**2)
      CF=2*P*F*WX/V
      WK=P/CF
      WRITE (6,20) THETA,F,W
      WRITE (6,25) N
      WRITE (6,30)
C     DO LOOP  TO DETERMINE UINC AND UREF AT EACH XN
      DO 15 I=40,200
      X=-2*WX+I*WX/50
      XN=X/WX
C     INTEGRATION PARAMETERS AND SUMMING VARIABLES
      SUM4=(0.0,0.0)
      SUM2=(0.0,0.0)
      FN=N
      H=2.0*WK/FN
      AX1=AI-WK
      AX2=AI+WK
      AX=AX1+H
      J=1
C     SUMMING ITERATIONS
   05 SUM4=SUM4+FNR(AX)*FNV(AX)*FNE(AX)
      SUM2=SUM2+FNR(AX+H)*FNV(AX+H)*FNE(AX+H)
      IF (J.GE.N-3) GO TO 10
      J=J+2
      AX=AX+2*H
      GO TO 05
```

```
   10   VR1=FNR(AX1)*FNV(AX1)*FNE(AX1)
        VR2=FNR(AX2)*FNV(AX2)*FNE(AX2)
        VR3=FNR(AX2-H)*FNV(AX2-H)*FNE(AX2-H)
        VR=(H/3)*(4*SUM4+2*SUM2+VR1+4*VR3+VR2)
        UREF=(CF**2/(4*P))*CABS(VR)**2
        UINC=EXP(-2*XN**2)
        WRITE (6,35) I,UINC,UREF
   15   CONTINUE
   18   CONTINUE
        STOP
   20   FORMAT (/2X,'THETA=',E10.4,2X,'FREQ=',E8.2,2X,'WIDTH='
   25   FORMAT (/5X,'INTERVAL NUMBER=',I8)
   30   FORMAT (/8X,'I',8X,'UINC',12X,'UREF'/)
   35   FORMAT (2X,I10,2E15.6)
        END
```

```
        COMPLEX FUNCTION FNR(AX)
        COMPLEX CI,A(3),B(3),BP,BM,T1,T2,T3
        DIMENSION V(3),ATT(3)
        P=3.141592654
        DI=0.8399832
        CI=(0.0,1.0)
C       SOUND VELS AND ATTENUATION CONSTANTS
        V(1)=1.48
        V(2)=2.74
        V(3)=1.35
        ATT(1)=0.00026/(2*P)
        ATT(2)=0.0271/(2*P)
        ATT(3)=0.0496/(2*P)
C       DO LOOPS FOR K'S AND KAPPAS
        DO 50 K=1,3
        A(K)=(V(1)/V(K))*CMPLX(1.0,ATT(K))
   50   CONTINUE
        DO 55 L=1,3
        BP=A(L)+AX
        BM=A(L)-AX
        PP=ATAN2(AIMAG(BP),REAL(BP))
        PM=ATAN2(AIMAG(BM),REAL(BM))
        IF (PP.LT.0.0)  PP=PP+2*P
        IF (PM.LT.0.0)  PM=PM+2*P
        B(L)=SQRT(CABS(BP)*CABS(BM))*CEXP(CI*(PP+PM)/2)
   55   CONTINUE
C       FUNCTION EVALUATION STEPS
        T1=(A(3)**2-2*AX**2)**2
        T2=4*B(2)*B(3)*AX**2
        T3=DI*(A(3)**4)*B(2)/B(1)
        FNR=(T1+T2-T3)/(T1+T2+T3)
        RETURN
        END
```

REFERENCES

1. A. Schoch, "Schallreflexion, Schallbrechnung und Schallbeugung", Ergeb. Exakt. Naturw. 23, 127-234 (1950).

2. H. L. Bertoni and T. Tamir, "Unified Theory of Rayleigh-Angle Phenomena for Acoustic Beams at Liquid-Solid Interface", J. Appl. Phys. 2, 157-172 (1973).

3. W. G. Neubauer, "Ultrasonic Reflection of a Bounded Beam at Rayleigh and Critical Angles for a Plane Liquid-Solid Interface", J. Appl. Phys. 44, 48-55 (1973).

4. F. L. Becker and R. L. Richardson, "Influence of Material Properties on Rayleigh Critical-Angle Reflectivity", J. Acoust. Soc. Amer. 51, 1609-1617 (1972).

5. L. E. Pitts, T. J. Plona and W. G. Mayer, "Theory of Non-Specular Reflection Effects for an Ultrasonic Beam Incident on a Solid Plate in a Liquid", IEEE Trans. SU. 24, 101-109 (1977).

6. H. L. Bertoni and Y. L. Hou, "Effects of Damping in a Solid on Acoustic Beams Reflected at the Rayleigh Critical Angle", Proc. 10th. Symp. NDE, San Antonio, Texas, 136-142 (1975).

7. M. A. Breazeale, L. Adler and G. W. Scott, "Interaction of Ultrasonic Waves Incident at the Rayleigh Angle onto a Liquid-Solid Interface", J. Appl. Phys. 48, 530-537 (1977).

8. L. M. Brekhovskikh, "Waves in Layered Media", Academic Press, New York, 1960.

9. L. E. Pitts, "A Unified Theoretical Description of Ultrasonic Beam Reflections from a Solid Plate in a Liquid", Ph.D. Thesis, Physics Department, Georgetown University, Washington, D.C., 1975.

10. C. E. Fitch, Jr., "New Methods for Measuring Ultrasonic Attenuation", J. Acoust. Soc. Amer. 40, 989-997 (1966).